Opposing effects of an F-box protein and the HSP90 chaperone network on microtubule stability and neurite growth in *Caenorhabditis elegans*

Chaogu Zheng[1,2,*], Emily Atlas[2], Ho Ming Terence Lee[1], Susan Laura Javier Jao[2], Ken C. Q. Nguyen[3], David H. Hall[3], and Martin Chalfie[2,*]

[1]School of Biological Sciences, The University of Hong Kong, Hong Kong SAR, China

[2]Department of Biological Sciences, Columbia University, New York, NY 10027, USA

[3]Department of Neuroscience, Albert Einstein College of Medicine, Bronx, NY 10461, U.S.A.

[*]Correspondence: cgzheng@hku.hk (C.Z.), mc21@columbia.edu (M.C.)

Key words: Neurite growth, microtubules, molecular chaperones, ubiquitination-proteasome system, protein homeostasis, touch receptor neurons

Running title: Opposing effects of UPS and chaperone

Summary statement: Molecular chaperones are known to protect cells from stress. However, in this study the authors showed that the Hsp90 chaperone negatively regulates neuronal differentiation when the ubiquitination-proteasome system is compromised.

Abstract

Molecular chaperones often work collaboratively with the ubiquitination-proteasome system (UPS) to facilitate the degradation of misfolded proteins, which typically safeguards cellular differentiation and protects cells from stress. In this study, however, we report that the Hsp70/Hsp90 chaperone machinery and an F-box protein, MEC-15, have opposing effects on neuronal differentiation and that the chaperones negatively regulate neuronal morphogenesis and functions. Using the touch receptor neurons (TRNs) of *Caenorhabditis elegans*, we find that *mec-15(-)* mutants display defects in microtubule formation, neurite growth, synaptic development, and neuronal functions, and these defects can be rescued by the loss of Hsp70/Hsp90 chaperones and cochaperones. MEC-15 likely functions in a SCF complex to degrade DLK-1, which is an Hsp90 client protein stabilized by the chaperones. The abundance of DLK-1, and likely other Hsp90 substrates, is fine-tuned by the antagonism between MEC-15 and chaperones; this antagonism regulates TRN development as well as synaptic functions of GABAergic motor neurons. Therefore, a balance between UPS and chaperones tightly controls neuronal differentiation.

Introduction

Molecular chaperones, including the heat shock proteins (Hsps), play essential roles in protein maturation, refolding, and degradation (Hartl et al., 2011; Lindquist and Craig, 1988). Although the function of Hsps in the response to stress has been extensively characterized, their roles in neuronal differentiation are much less understood. Ishimoto et al. (1998) found that Hsp90 promotes neurite extension for the chick telencephalic neurons and spinal neurons *in vitro*. More recently, pharmacological inhibition of Hsp90 by 17-demethoxygeldanamycin (17-AAG) disturbed neuronal polarization and axonal elongation of cultured hippocampal neurons (Benitez et al., 2014). Hsp90 inhibition decreased expression of two Hsp90 client proteins, Akt and GSK3, which have diverse functions in cell differentiation. Thus, Hsp90 may regulate axon specification and growth by affecting specific signaling pathways through its chaperone activity. Given that the Hsp70 and Hsp90 chaperones interact with numerous client proteins, including transcription factors, kinases, and signaling molecules (Wayne et al., 2011), the regulation of neuronal morphogenesis by the chaperones is likely to be context-dependent. Whether Hsp70 and Hsp90 chaperones and their co-chaperones can also negatively regulate neurite growth, however, is unclear.

The ubiquitination-proteasome system (UPS) often works in concert with the chaperone-mediated refolding machinery for protein quality control, which promotes degradation of numerous misfolded proteins in a chaperone-dependent manner (Buchberger et al., 2010). In developing neurons, this process safeguards the protein quality of important guidance molecules. For example, in *Caenorhabditis elegans* the BC-box protein EBAX-1, the substrate-recognition subunit of the Elongin BC-containing Cullin-RING ubiquitin ligase (CRL), and HSP-90/Hsp90 collaboratively regulate the folding and degradation of misfolded SAX-3/Robo receptor during axonal pathfinding (Wang et al., 2013). By preferentially binding to misfolded SAX-3, EBAX-1 not only recruits Hsp90 to promote the refolding of nonnative SAX-3 but also mediates the degradation of irreparable SAX-3 through CRL activity.

Despite known examples of collaboration, UPS and molecular chaperones could theoretically have opposing effects as well, since UPS increases normal protein turnover and chaperones can enhance protein stability. The antagonism of the UPS and the molecular chaperone machinery during neuronal differentiation, however, has not, to our knowledge, been

91 previously reported.

92 In this study, we find that the F-box and WD40 repeat domain-containing protein
93 MEC-15 (an ortholog of human FBXW9) and ubiquitination promote microtubule (MT)
94 stability and neurite growth by countering the activity of the Hsp70/Hsp90 chaperone network.
95 Mutations in *mec-15* led to a range of developmental defects in the *C. elegans* touch receptor
96 neurons (TRNs), including the loss of microtubules (MTs), inhibited neurite growth and
97 branching, defects in localizing synaptic proteins, and the loss of sensory function. All these
98 defects in *mec-15* mutants can be rescued by removing the Hsp70 and Hsp90 chaperones and
99 co-chaperones, which unexpectedly suggests that the chaperones can disrupt neurite growth
100 and neuronal development and this activity is normally suppressed by the F-box protein and
101 the ubiquitination pathway. Downstream of the chaperones, we identified the MAP3 kinase
102 DLK-1 as an Hsp90 client protein that has MT-destabilizing activity and can inhibit neurite
103 growth. Therefore, our studies provided an important example of how the effects of molecular
104 chaperones are opposed by the ubiquitination pathway during neuronal differentiation.

105

106 **Results**

107 **The F-box protein MEC-15 is required for MT stability and neurite growth**

108 The six *C. elegans* touch receptor neurons (ALML/R, PLML/R, AVM, and PVM) are
109 mechanosensory neurons that respond to gentle touch and have a simple morphology (Figure
110 1A-B). We previously identified a set of neomorphic tubulin mutations that caused the
111 formation of hyperstable MTs and the growth of an ectopic, posteriorly directed neurite in ALM
112 neurons (termed ALM-PN; similarly, ALM-AN is the anteriorly directed neurite of ALM;
113 PLM-AN and PLM-PN are the anteriorly and posteriorly directed neurites of PLM,
114 respectively; Zheng et al., 2017). Among those mutants, the β-tubulin *mec-7(u278;* C303Y*)*
115 allele had the strongest phenotype, with a very long ALM-PN extending to the tail region. By
116 suppressing this *mec-7(neo)* phenotype, we sought to identify genes that regulate MT stability
117 and neurite development. This *mec-7(u278)* suppressor screen (see Materials and Methods)
118 yielded a *mec-15* nonsense allele *u1042(*R26**)*, which completely suppressed the growth of
119 ALM-PN in *mec-7(u278)* mutants. Another *mec-15* loss-of-function *(lf)* allele *u75(*Q118**)*
120 showed similar suppression (Figure 1A-B and 2A). *mec-15* codes for a protein that contains a

121 N-terminal F-box and four WD-40 repeats (Figure 1C; Bounoutas et al., 2009b) and is
122 orthologous to human FBXW9.

123 The loss of *mec-15* also suppressed the growth of ectopic ALM-PN induced by other
124 mutations that increased MT stability and caused the formation of an ALM-PN (Figure 1D),
125 including another neomorphic β-tubulin mutation *mec-7(u1017;* L377F*)*, a *lf* mutation in a
126 destabilizing α-tubulin gene *tba-7*, and a *lf* mutation in a MT-depolymerizing kinesin-13 gene
127 *klp-7* (Zheng et al., 2017). These data suggest that MEC-15, a F-box protein, is generally
128 required for the excessive neurite growth triggered by elevated MT stability in TRNs.

129 MEC-15 is also required for normal TRN morphology. *mec-15(lf)* alleles *u75* and
130 *u1042* caused the shortening of both PLM-AN and PLM-PN in an otherwise wild-type
131 background (Figure 1E, 2D, and S1). Another *mec-15* nonsense allele *u1008(*Q194***)*, isolated
132 from a different screen (Zheng et al., 2017), showed similar TRN morphological defects
133 (Figure S1A-C). Previous studies found that *mec-15* is required for touch sensitivity and the
134 localization of presynaptic proteins in TRNs (Bounoutas et al., 2009b). We found that the
135 ALM-AN and PLM-AN in *mec-15* mutants could not fully extend their synaptic branches
136 (Figure 1E, iv and v), which may have caused the synaptic defects.

137 As previously found (Bounoutas et al., 2009b; Sun et al., 2013), a *mec-15::GFP*
138 translational reporter was expressed in the TRNs, several head and tail neurons, and ventral
139 cord motor neurons (Figure 1F). We also generated a *mec-15::GFP* knock-in allele at the
140 endogenous *mec-15* locus through CRISPR/Cas9-mediated gene editing, but the resulting
141 strain did not have any detectable GFP expression, suggesting that the endogenous MEC-15
142 level may be quite low. We next tested whether MEC-15 functions cell-autonomously in the
143 TRNs. Expression of wild-type *mec-15(+)* from the TRN-specific *mec-18* promoter rescued
144 both the neurite growth defects in *mec-15(-)* single mutants and the loss of ALM-PN in *mec-*
145 *15(-); mec-7(u278 neo)* double mutants. In contrast, the expression of MEC-15 with some or
146 all of the F-box domain removed could not rescue either phenotype (Figure 1D and S1A-C),
147 suggesting that MEC-15 functions within the TRNs and its activity requires the F-box domain.

148 F-box proteins assemble with Skp and Cullin proteins to form SCF E3 ubiquitin ligase
149 complexes. The involvement of ubiquitination in the action of MEC-15 was supported by the
150 findings that TRN-specific knockdown of *uba-1*, the only known *C. elegans* gene encoding a

151 ubiquitin-activating enzyme, strongly suppressed the growth of ALM-PN in *mec-7(u278 neo)*
152 mutants (Figure S1D). Because mutation or general knockdown of *uba-1* causes sterility and
153 lethality, we performed cell-specific RNAi by expressing double-stranded RNA (dsRNA)
154 against *uba-1* from the TRN-specific *mec-17* promoter. As a negative control, expression of
155 dsRNA against GFP did not affect neurite growth. Moreover, inhibition of proteasomes by
156 bortezomib partially suppressed the growth of ALM-PN (Figure S1D). In addition, previous
157 work found that MT depolymerization led to a general reduction in protein levels in TRNs
158 (Bounoutas et al., 2011). We found that mutations in *mec-15*, knockdown of *uba-1*, and
159 bortezomib treatment all significantly reduced TagRFP expression from a *mec-17p::TagRFP*
160 transgene in the TRNs, measured as fluorescent intensity (Figure S1E). The above data lead to
161 the hypothesis that some MT-destabilizing molecule, which is normally ubiquitinated and
162 targeted for degradation by MEC-15, accumulated abnormally in the *mec-15*-deficient TRNs,
163 leading to reduced MT stability and the inhibition of neurite growth.

164 Although reduced *uba-1* activity affected ALM-PN outgrowth, we could not identify
165 the other components of the putative SCF complex. In fact, our results suggest that these other
166 components may be redundant. For example, although we found that MEC-15 physically
167 interacted with the Skp homolog SKR-1 in a yeast two-hybrid assay (Figure S1F), *skr-1(ok1696)*
168 null mutations neither caused TRN morphological defects nor suppressed ALM-PN outgrowth
169 in *mec-7(u278 neo)* mutants. In addition, RNAi of *skr-2, skr-8, skr-9, skr-12,* and *skr-13* (other
170 Skp homologs) did not suppress the Mec-7(neo) phenotype (see Materials and Methods for
171 details). Cullin, the third component of the SCF complex, also appeared to be redundant, since
172 mutations or knockdown of Cullin homologs *cul-1*, *cul-2*, *cul-4*, *cul-5*, and *cul-6* did not induce
173 the same defect as the loss of MEC-15.

174 **Loss of molecular chaperones suppresses neurite growth defects of *mec-15* mutants**

175 To identify the downstream target(s) of the MEC-15-dependent ubiquitination
176 pathway, we screened for suppressors of *mec-15* in the *mec-15(u1042); mec-7(u278)*
177 background and identified the phenotype-causing mutations in eight mutants with restored
178 ectopic ALM-PNs (Table S1; see Materials and Methods for details). Among those mutants
179 were one recessive *lf* allele of *sti-1* and four recessive *lf* alleles of *pph-5*. *sti-1* encodes a
180 homolog of the Sti1/Hop cochaperone that physically links Hsp70 and Hsp90 through the

181 tetratricopeptide repeat (TPR)-domain (Schmid et al., 2012), and *pph-5* encodes a homolog of
182 Protein Phosphatase 5 (PP5), a TPR-domain containing serine/threonine phosphatase that binds
183 to Hsp90 and activates its kinase clients (Vaughan et al., 2008). Deletion alleles of either genes
184 [*sti-1(ok3354)* and *pph-5(ok3498)*] also induced the growth of ALM-PN in *mec-15(u1042);*
185 *mec-7(u278)* animals (Figure 2A-C and Table S1).

186 Since STI-1 and PPH-5 are components of the molecular chaperone pathway, we
187 tested other genes in the same pathway. The removal of *hsp-90* (a Hsp90 homolog) and *hsp-*
188 *110* (a Hsp70 family member) but not *hsp-1* (another Hsp70 family protein) suppressed the loss
189 of MEC-15. *hsp-90(ok1333)* and *hsp-110(gk533)* deletion alleles caused larval arrest, but the
190 arrested *mec-15(u1042); hsp-90(ok1333); mec-7(u278)* and *mec-15(u1042); hsp-110(gk533);*
191 *mec-7(u278)* triple mutants had long ALM-PNs (Figure 2C).

192 Moreover, TRN-specific knockdown of *hsf-1*/heat shock transcription factor 1, which
193 activates the expression of Hsps and functions upstream of HSP-90 and HSP-110 (Singh and
194 Aballay, 2006), also induced the growth of ALM-PNs in *mec-15(u1042); mec-7(u278)* double
195 mutants (Figure 2C). PP5, the PPH-5 homolog, dephosphorylates the co-chaperone Cdc37 in
196 yeast and mammals, which is essential for the folding and maturation of Hsp90-dependent
197 protein kinases (Vaughan et al., 2008; Wandinger et al., 2006). TRN-specific RNAi silencing
198 of *cdc-37*, *C. elegans* Cdc37, promoted the growth of ALM-PN in *mec-15(-); mec-7(u278)*
199 animals (Figure 2C), suggesting that some Hsp90 kinase clients may be involved in the
200 regulation of neurite growth.

201 Through a candidate RNAi screen of 27 Hsp70/Hsp90-related genes (Table S2), we
202 found that knocking down *daf-41*, which encodes the Hsp90 co-chaperone PTGES3/p23, also
203 restored the growth of ALM-PNs in *mec-15(u1042); mec-7(u278)* animals (Figure S2C). A
204 *daf-41* deletion allele, *ok3052*, produced the same phenotype (Figure 2C). Thus, disrupting the
205 Hsp70/Hsp90 chaperone machinery by deleting Hsp70, Hsp90, p23, Sti1/Hop, PP5, or Cdc37
206 rescued the loss of the F-box protein MEC-15.

207 Importantly, the suppression of *mec-15* loss did not depend on the presence of *mec-*
208 *7(u278 neo)*. We crossed *lf* alleles of *hsp-110*, *hsp-90*, *daf-41/p23*, *sti-1*, and *pph-5* with *mec-*
209 *15(u1042)* to create double mutants and found that the shortening of PLM-PN in *mec-15* single
210 mutants was suppressed in all double mutants (Figure 2E and G). TRN-specific knockdown of

211 *cdc-37* had similar effects (Figure 2G). In addition, we found that the PLM-AN outgrowth
212 defect (but not that of PLM-PN) in *mec-15* null mutants was more severe at 25°C than at 20°C
213 (Figure S2A and S2B), suggesting that the abnormally accumulated proteins may have higher
214 expression or exert a stronger MT-destabilizing activity at higher temperature. This more
215 severe PLM-AN growth defect at 25°C was also suppressed in *mec-15; daf-41*, *mec-15; sti-1*,
216 and *mec-15; pph-5* double mutants; most PLM-ANs extended fully and grew beyond the vulva
217 (Figure 2F). We could not measure the length of PLM-AN in *mec-15; hsp-110* and *mec-15;*
218 *hsp-90* adults, because those double mutants arrested at early larval stages.

219 HSP-90 and the cochaperones DAF-41, STI-1, and PPH-5 are expressed in most *C.*
220 *elegans* cells (Gillan et al., 2009; Richie et al., 2011; Song et al., 2009), and we confirmed their
221 expression in the TRNs (Figure S3A-C). Moreover, we were able to rescue the loss of *daf-41*,
222 *sti-1*, and *pph-5* in their double mutants with *mec-15(u1042)* and their triple mutants with *mec-*
223 *15(u1042); mec-7(u278)* by expressing the wild-type cochaperone gene from a TRN-specific
224 *mec-17* promoter, indicating that the chaperone pathway genes function cell-autonomously in
225 the TRNs (Figure S3D). Unexpectedly, mutants of chaperones and cochaperones also had
226 strong maternal effects in suppressing the *mec-15*(-) phenotype (Figure S4; see Supplemental
227 Results for details).

228 Moreover, *hsp-110*, *hsp-90*, *daf-41*, *sti-1*, and *pph-5* single mutants did not show any
229 TRN morphological defects (Figure S5) and *daf-41*, *sti-1*, and *pph-5* single mutants did not
230 cause touch insensitivity (Figure 4G; we could not test *hsp-110* and *hsp-90* homozygous
231 mutants, which are quite uncoordinated and unhealthy and arrest at larval stages). These results
232 suggest that their activities are normally not required for TRN differentiation and function.
233 Nevertheless, an inhibitory role for these Hsp70/Hsp90 chaperones and cochaperones on TRN
234 differentiation is revealed when *mec-15* is lost, because the chaperone proteins were required
235 for the disruption of TRN morphology and functions in *mec-15(-)* mutants.

236 **Phosphorylation of STI-1 inhibits its activity in regulating neurite growth**

237 Because mutations in *pph-5* and *sti-1* showed the strongest and almost identical effects
238 in suppressing *mec-15(-)* phenotype, we wondered whether, in addition to activating Hsp90
239 and Cdc37, PPH-5 may also activate STI-1 activity through dephosphorylation. This
240 hypothesis is based on previous findings that the phosphorylation of yeast Sti1 and human Hop,

241 STI-1 homologs, appeared to inhibit its cochaperone activity (Rohl et al., 2015).

242 Both yeast and human Sti1/Hop proteins contain three TPR domains and two DP
243 (aspartate and proline rich) domains; the TPR2A domain interacts with Hsp90, whereas the
244 TPR1 and TPR2B domains interact with Hsp70 (Schmid et al., 2012). Although *C. elegans*
245 STI-1 contains only TPR2A and TPR2B and one DP domain (Figure 3A), STI-1 is likely
246 capable of transferring clients from Hsp70 and Hsp90. Yeast and human Sti1/Hop proteins
247 contain six and five phosphorylation sites, respectively, which are found mostly flanking the
248 Hsp70-interacting TPR1 and TPR2B domains or in the linker region; those sites are not
249 conserved and appear to be unique to the species (Rohl et al., 2015). Similarly, we predicted
250 potential phosphorylation sites in *C. elegans* STI-1 flanking TPR2B and in the linker region,
251 as well as the only phosphorylatable residue (S289) in the DP domain (Figure 3A); those sites
252 are mostly unique to *C. elegans* STI-1, except Y134 and Y163, which are conserved among
253 yeast, human, and *C. elegans*.

254 We reasoned that if PPH-5 regulated STI-1 activity through dephosphorylation, *pph-*
255 *5(-)* mutants might have hyperphosphorylated STI-1 with low activity and the expression of
256 non-phosphorylatable STI-1 in *pph-5* mutants might rescue STI-1 activity and thus suppress
257 the loss of *pph-5*. Indeed, TRN-specific expression of non-phosphorylatable STI-1 mutants that
258 removed one or several potential modification sites suppressed the effect of *pph-5(-)* mutation
259 to varying degrees in *mec-15(u1042); mec-7(u278)* animals (Figure 3B). As a control,
260 overexpression of wild-type STI-1 had little effect on ALM-PN growth in *pph-5; mec-15; mec-*
261 *7* animals (Figure 3B). Among the STI-1 mutants, S240A-S254A and Y134F-S289A most
262 strongly suppressed the rescuing effects of *pph-5(-)* mutations on ALM-PN growth, suggesting
263 that 1) those residues are key regulatory sites on STI-1; and 2) PPH-5 functions to activate STI-
264 1. We should point out that PPH-5 is serine/threonine phosphatase and cannot dephosphorylate
265 phospho-tyrosine. So, the inhibitory effect on the tyrosine-to-phenylalanine changes on ALM-
266 PN growth may result from the reduction of overall phosphorylation level of STI-1 and was
267 not specific to the loss of *pph-5*. PPH-5 likely acts through S240, S254, and S289 but not Y134.

268 Overexpression of STI-1(Y134F-S289A) mutants in *mec-7(u278)* animals also
269 strongly suppressed the growth of ectopic ALM-PN (Figure 3C), indicating that STI-1
270 dephosphorylation can significantly elevate its activity in destabilizing MTs and inhibiting

271 neurite growth. Consistent with this notion, overexpression of phosphomimic and inactive STI-
272 1 mutants (e.g. S240E-S254E) in *mec-15(u1042); mec-7(u278)* partially suppressed *mec-15(-)*
273 mutation and restored ALM-PN in *mec-15; mec-7* animals presumably by competing with
274 endogenous STI-1 (Figure 3D). The above data indicate that, similar to yeast and mammalian
275 Sti1/Hop proteins, *C. elegans* STI-1 is regulated by inhibitory phosphorylation, and PPH-5 may
276 activate STI-1 through dephosphorylation.
277
278 **Mutations in chaperones rescues MT loss and synaptic defects of *mec-15* mutants**
279 Consistent with the hypothesis that chaperones are detrimental for TRN development
280 in *mec-15* mutants, we also observed suppressing effects of chaperone mutations on *mec-15(-)*-
281 induced changes in MT organization. We previously showed that MT organization and stability
282 determined neurite growth patterns in TRNs (Zheng et al., 2017). Using electron microscopy
283 (EM), we found that the number of MTs in a cross section of TRN neurite is dramatically
284 reduced in *mec-15* mutants compared to the wild type in both ALM and PLM (Figure 4A-B).
285 For example, PLM-AN in *mec-15(u1042)* mutants had 4.9 ± 2.9 (mean ± SD) MTs on average
286 in a cross section, compared to 29.8 ± 6.5 MTs in the wild type. In addition to the loss of MTs,
287 *mec-15* mutants also had smaller MTs than the wild type. For example, whereas 98% (N = 306)
288 of the MTs in the wild type had the 15-protofilament (15-p) MTs, 71% (N = 65) of the MTs in
289 the PLM-AN of *mec-15(u1042)* adults had between 11 and 13 protofilaments, resulting in
290 significantly smaller MT diameters (Figure 4C-D). The loss of MTs and the smaller size
291 indicate that MTs are highly unstable and disorganized in the absence of MEC-15.
292 The structural defects of MTs in *mec-15* mutants are rescued in *mec-15; sti-1* and *mec-*
293 *15; pph-5* double mutants, which had restored MT numbers, 16.2 ± 4.3 and 17.6 ± 9.2 MTs in
294 the PLM-AN, respectively. The double mutants also have large-diameter 15-protofilament MTs,
295 similar to those seen in the wild type (Figure 4D). These data suggest that the loss of Hsp90
296 co-chaperones promotes MT formation and stability, which in turn rescues the TRN neurite
297 growth defects in *mec-15* mutants.
298 Consistent with our previous finding that MT depolymerization in the TRNs causes a
299 general reduction in protein levels (Bounoutas et al., 2011), *mec-15* mutants showed drastically
300 decreased TagRFP expression from a *mec-17p::TagRFP* transgene in the TRNs, compared to

301 the wild type (Figure 4E). This reduction in protein level was completely rescued by mutations
302 in *daf-41/p23*, *sti-1*, and *pph-5* (Figure 4E). Moreover, *mec-15* mutants also showed almost
303 complete loss of GFP::RAB-3 localization at the presynaptic site in PLM neurons and partial
304 loss in ALM neurons (Bounoutas et al., 2009b). This transport defect is likely caused by
305 unstable MTs and is suppressed by the mutations in *sti-1* and *pph-5* (Figure 4F).

306 TRNs are mechanosensory neurons that detect gentle touch to the body; this sensory
307 function of TRNs depends on the 15-p MTs (Bounoutas et al., 2009a). Mutations in *mec-15*
308 cause touch insensitivity (Chalfie and Au, 1989), likely due to the loss of 15-p MTs. This
309 sensory defect was fully rescued in *sti-1; mec-15* and *pph-5; mec-15* double mutants and
310 partially rescued in *daf-41; mec-15* double mutants (Figure 4G).

311 Thus, in addition to neurite development, the removal of the molecular chaperone
312 pathway genes restored a variety of MT-related structures and functions affected by *mec-15*
313 loss. Given the protective nature of the chaperones, this restoration is rather unexpected and
314 suggests that Hsp70/Hsp90 machinery may contribute to the refolding and stabilization of a
315 client protein or proteins that negatively affects MT stability and TRN development.

316 **Hsp90 chaperones inhibit neurite growth by stabilizing DLK-1**

317 Since our *mec-15* suppressor screen (Table S1) yielded two *dlk-1 lf* alleles, *u1105*
318 (V844I) and *u1138* (W394*), we examined the possibility that Hsp70/Hsp90 might regulate
319 MT organization and neurite growth by acting on *dlk-1*, which encodes a MAP3 kinase
320 homologous to human MAP3K12 and MAP3K13. Both *u1105* and *u1138* mutations restored
321 the growth of both ALM-PN and PLM-PN in *mec-15(u1042); mec-7(u278)* mutants (Figure
322 5A and B). The missense mutation (V844I) in *u1105* is adjacent to a C-terminal region (aa 850-
323 881) of DLK-1 that interacts with its kinase domain (Yan and Jin, 2012); so, catalytic function
324 of DLK-1 may be impaired in *u1105* mutants. Another *dlk-1 lf* allele, *ju476* (a frameshift
325 mutation), suppressed *mec-15(-)* even more strongly. The phenotype of *dlk-1(-)* is similar to
326 the effects of *sti-1(-)* and *pph-5(-)* in *mec-15; mec-7* mutants. Independent of the *mec-7(u278)*
327 background, *dlk-1 lf* alleles also suppressed the shortening of PLM-PN and the premature
328 termination of PLM-AN in *mec-15(u1042)* mutants (Figure 5C and D). Moreover, *dlk-1 lf*
329 alleles showed maternal effects similar to *daf-41*, *sti-1,* and *pph-5 lf* alleles (Figure 5B). These
330 data suggest that *dlk-1* may function in the same pathway as the chaperone and co-chaperone

331 genes.

332 Expression of DLK-1a from the TRN-specific *mec-17* promoter rescued the loss of
333 *dlk-1* by suppressing the growth of ALM-PN in *dlk-1; mec-15; mec-7* triple mutants,
334 confirming that DLK-1 functions cell-autonomously (Figure 5E). More importantly,
335 overexpression of DLK-1a also suppressed the phenotype of *pph-5* and *sti-1* mutants,
336 indicating that DLK-1 functions downstream of the chaperones (Figure 5E). Through a yeast
337 two-hybrid assay, we detected a physical interaction between HSP90 and DLK-1a (Figure 5F),
338 which is the long and active isoform of DLK-1 (Yan and Jin, 2012). Moreover, the level of
339 GFP::DLK-1a fusion protein is drastically reduced in *pph-5* and *sti-1* mutants, suggesting that
340 the stability of DLK-1 relies on the Hsp90 chaperones (Figure 5G).

341 DLK-1 is known to induce MT dynamics and is essential for axonal regeneration in
342 TRNs (Tang and Chisholm, 2016; Yan et al., 2009); DLK-1 signaling is also required for MT
343 depolymerization-induced downregulation of protein levels in TRNs (Bounoutas et al., 2011).
344 Indeed, *dlk-1 lf* mutations blocked the downregulation of TagRFP in *mec-15(-)* animals, while
345 overexpression of DLK-1a in the wild-type animals led to marked reduction of TagRFP
346 expression (Figure 5H). Consistent with a role in reducing MT stability, DLK-1a
347 overexpression strongly suppressed the growth of ectopic ALM-PN in *mec-7(u278)* animals
348 and also shortened PLM-AN and PLM-PN in wild-type animals (Figure 5C and E). The above
349 data suggest that DLK-1 likely mediates the activity of Hsp90 chaperones and cochaperones in
350 destabilizing MTs during development. Coincidentally, a recent study found that Hsp90 is also
351 a chaperone for DLK in mouse neurons and in Drosophila and is required for axon injury
352 signaling (Karney-Grobe et al., 2018). Thus, the regulation of DLK-1 by Hsp90 chaperone
353 appears to be evolutionarily conserved.

354 Importantly, DLK-1 is not the only downstream effector of the chaperones, because
355 unlike the *sti-1* and *pph-5 lf* mutations, the *dlk-1 lf* mutations did not rescue the touch
356 insensitivity, PLM-AN branching defects, or the GFP::RAB-3 localization defect in *mec-15*
357 mutants (Figure S6). Even for neurite growth, the loss of *dlk-1* did not fully rescue the
358 outgrowth defect of PLM-PN and PLM-AN in *mec-15* mutants (Figure 5C and D). Thus, we
359 expect that other Hsp90 client proteins also function during TRN development.

360 **MEC-15 downregulates DLK-1 levels in TRNs**

361 Since MEC-15 is a F-box protein that likely functions in a SCF complex to target
362 substrate protein for ubiquitination and degradation, we next asked whether MEC-15 regulates
363 DLK-1 protein levels. We found that the expression of GFP::DLK-1 fusion proteins was
364 elevated in *mec-15* mutants (Figure 5G), whereas the levels of STI-1::GFP and PPH-5::GFP
365 fusion proteins were not changed in *mec-15* mutants (Figure S7A). Importantly, the level of
366 GFP::DLK-1 was also increased by blocking ubiquitination through TRN-specific silencing of
367 *uba-1* (Figure 5G). Thus, MEC-15 likely targets DLK-1 but not the Hsp90 co-chaperones for
368 degradation.

369 We could not detect any physical interaction of MEC-15 with DLK-1a in yeast two-
370 hybrid assays, suggesting that the interaction may be transient or dependent on particular post-
371 translational modification of DLK-1. We did not detect any interaction of MEC-15 with STI-
372 1, PPH-5, DAF-41, HSP-90, or HSP-110 either. In attempts to detect MEC-15 binding to DLK-
373 1 in the TRNs, we made constructs that express HA-tagged MEC-15 and FLAG-tagged DLK-
374 1 from the TRN-specific *mec-18* and *mec-17* promoters, respectively. When we injected the
375 two expression constructs into worms separately, both MEC-15 and DLK-1 can be detected by
376 western blot probing the tags; but when injected together, only MEC-15::HA was detected, and
377 FLAG::DLK-1 was undetectable (Figure S7B). Although this renders the co-
378 immunoprecipitation assay impossible, these results suggested that MEC-15 suppressed the
379 expression of DLK-1 protein.

380 RPM-1, a RING-finger E3 ubiquitin ligase, also downregulates the abundance of
381 DLK-1 at the protein level and modulates the p38 MAP Kinase pathway (Nakata et al., 2005).
382 The phenotype of *rpm-1* mutants, however, is the direct opposite of *mec-15* mutants. Instead
383 of the shortened TRN neurites of *mec-15* mutants, *rpm-1(ok364)* knockout mutants had
384 overextended ALM-AN and PLM-AN (Figure S7C; Schaefer et al., 2000). Moreover, the loss
385 of *rpm-1* did not suppress the ectopic ALM-PN in *mec-7(u278)* mutants, and the *rpm-1 mec-7*
386 double mutants showed both long ALM-PN and the overextension of ALM-AN and PLM-AN
387 (Figure S7D-F). Thus, RPM-1 appears to negatively regulate neurite growth, whereas MEC-
388 15 promotes growth. Downstream of both proteins, DLK-1 may exert dual functions in both
389 inducing MT dynamics and promoting neurite extension depending on the cellular contexts.

390 *mec-15* is epistatic to *rpm-1*, since *mec-15; rpm-1* double mutants showed mostly the

391 *mec-15(-)* phenotype, having shortened PLM-ANs and PLM-PNs. The *mec-15; rpm-1; mec-7*
392 triple mutants showed the phenotype of *mec-15; mec-7* double mutants in the suppression of
393 ALM-PN (Figure S7E-F). This epistasis suggests that either MEC-15-mediated regulation of
394 DLK-1 plays a more dominant role in TRNs than RPM-1-mediated regulation or MEC-15-
395 regulated DLK-1-independent pathways act downstream of RPM-1.

396 **MEC-15 regulates the function of GABAergic motor neuron by antagonizing Hsp90**
397 **chaperone activities**

398 Finally, the genetic interaction between *mec-15* and the Hsp90 chaperones occurs not
399 only in the TRNs, but also in other neurons. In the ventral cord motor neurons, MEC-15
400 regulates the trafficking of synaptic vesicle protein SNB-1 and promotes GABAergic synaptic
401 transmission (Sun et al., 2013). We found that *mec-15* mutants had fewer synaptic puncta
402 labeled by SNB-1::GFP in GABAergic neurons than wild-type animals (Figure 6A-C). This
403 deficit in synaptic density was rescued by mutations in *sti-1* or *pph-5*, although the average
404 fluorescent intensity of each puncta was similar between the mutants and the wild-type animals
405 (Figure 6A-C).

406 Behaviorally, reduced GABA release in *mec-15* mutants led to lower inhibitory
407 postsynaptic currents in the body wall muscles and increased sensitivity to the acetylcholine
408 esterase inhibitor aldicarb, which causes paralysis through the accumulation of acetylcholine
409 and persistent muscle contraction (Sun et al., 2013). This increased sensitivity to aldicarb in
410 *mec-15* mutants was completely suppressed in *mec-15; sti-1* and *mec-15; pph-5* mutants
411 (Figure 6D). Therefore, MEC-15 and Hsp90 chaperones also appear to counter each other to
412 regulate GABAergic synaptic function. Moreover, similar to the thermosensitive PLM-AN
413 growth defects in *mec-15* mutants, we found that *mec-15(-)* animals grown at 25°C are much
414 more sensitive to aldicarb than animals raised at 20°C; loss of *sti-1* or *pph-5* also rescued this
415 temperature-dependent defects (Figure 6D). These results suggest that MEC-15 target proteins
416 in both TRNs and GABAergic motor neurons are more stable or have higher levels at higher
417 temperature, likely due to the increased activity of Hsp90 chaperones at higher temperature.
418

419 **Discussion**

420 **Ubiquitination and protein degradation promote stable MTs and neurite growth**

421 The ubiquitination-proteasome system (UPS) affects many processes of neuronal
422 development, including neurogenesis, cell fate specification, neuronal migration, polarization,
423 and axonal and dendrite morphogenesis (Tuoc and Stoykova, 2010; Yamada et al., 2013). With
424 respect to neurite morphogenesis, previous studies suggested that E3 ubiquitin ligase can both
425 positively and negatively regulate neurite growth. For example, during axodendritic
426 polarization in hippocampal neurons, the HECT-domain E3 ubiquitin ligase Smurf1 promotes
427 the growth of axons by degrading RhoA (inhibitor of axon growth), whereas Smurf2 inhibits
428 the growth of neurites fated to be dendrites by degrading Ras GTPase Rap1B (inducer of
429 neurite growth; Cheng et al., 2011; Schwamborn et al., 2007).

430 Our studies identified the F-box and WD40 domain protein MEC-15 (ortholog of
431 human FBXW9) as a positive regulator of neurite growth. As in the above examples, MEC-15
432 presumably functions in a Skp, Cullin, F-box containing complex (or SCF complex), which is
433 a E3 ubiquitin ligase, to degrade some protein(s) that can inhibit neurite outgrowth. One
434 potential substrate of MEC-15 is the MAP3 kinase DLK-1, which is known to induce MT
435 dynamics (Tang and Chisholm, 2016) and can suppress neurite growth when overexpressed
436 (this study). Since the loss of *dlk-1* did not fully rescue the developmental defects of *mec-15(-)*
437 mutants, MEC-15 likely has multiple substrates.

438 In the PLM neurons, the anterior neurite is considered an axon because its MTs has
439 uniform "plus-end out" polarity, whereas the posterior neurite is more like a dendrite given that
440 its MTs have mixed polarity (Hsu et al., 2014). MEC-15 is required for the extension of both
441 PLM-AN and PLM-PN, which suggests that MEC-15 is a general regulator of neurite growth
442 instead of an axon- or dendrite-specific regulator, like the E3 ligase Cdh1-APC and Cdc20-
443 APC (Konishi et al., 2004). This function of MEC-15 may be attributed to its activity in
444 promoting the formation of stable MTs, since mutations in *mec-15* led to significant loss of
445 MTs and the reduction of MT diameters. Thus, our studies link SCF complex and UPS to the
446 general stability of MT cytoskeletons.

447 **Dual yet contradictory functions of DLK-1**

448 Another conserved RING-domain E3 ubiquitin ligase, RPM-1, also regulates neurite
449 extension in TRNs by interacting with the SCF complex, including SKR-1/Skp, CUL-1/Cullin,
450 and the F-box protein FSN-1/FBXO45 (Nakata et al., 2005). However, MEC-15 and RPM-1

451 have opposing functions. MEC-15 promotes neurite growth, whereas RPM-1 inhibits neurite
452 growth. More surprisingly, both RPM-1 and MEC-15 appear to target DLK-1 for degradation.
453 Since mutations in *dlk-1* partially suppress both the overextension phenotype in *rpm-1(-)*
454 mutants (Nakata et al., 2005) and the underextension in *mec-15(-)* mutants (this study), DLK-
455 1 may exhibit dual yet opposite functions in regulating neurite growth.

456 Elevated DLK-1 level promotes axon growth in *rpm-1(-)* mutants but inhibits neurite
457 growth in *mec-15(-)* mutants; these two opposing functions seem to be balanced under normal
458 conditions, since *dlk-1(-)* mutants did not show any TRN morphological defects. Perhaps the
459 spatial and temporal expression of DLK-1 determines which of the two opposing functions is
460 engaged. For example, DLK-1 may play inhibitory roles for general neurite extension during
461 the growth phase by reducing MT stability globally in the entire cell and then prevent axon
462 termination at specific sites at a later stage of development. Because *mec-15(-) rpm-1(-)* double
463 mutants exhibited the underextension phenotype, the overall effects of accumulating DLK-1
464 appear to inhibit neurite growth. Interestingly, DLK-1 also initiates apparently contradictory
465 responses under stress conditions during development and after axonal injury (Tedeschi and
466 Bradke, 2013). For example, after optical nerve injury in mice, DLK triggers the expression of
467 both proapoptotic and regenerative genes, although cell death is the dominant response
468 (Watkins et al., 2013). Future studies are needed to understand how the multifaceted functions
469 of DLK-1 are controlled spatially and temporally to initiate specific signalling. Our work also
470 suggests that different components of the UPS could generate distinct cellular responses by
471 targeting the same protein.

472 **Inhibitory role of Hsp70/Hsp90 chaperones and co-chaperones in neuronal development**

473 Besides the protective effects of Hsps in cells under stressed conditions, growing
474 evidence suggest that these chaperones also play regulatory roles in normal neurodevelopment
475 (Miller and Fort, 2018). The ATP-dependent Hsp70 and Hsp90 family chaperones are
476 expressed in the nervous system during mouse embryonic and postnatal development, which
477 suggests that they may function in both neurogenesis and late-stage neurodevelopment (Loones
478 et al., 2000). In fact, deletion of the transcription factor HSF1, which activates the transcription
479 of many Hsp genes, led to impaired olfactory neurogenesis and hippocampal spinogenesis and
480 neurogenesis in mice (Uchida et al., 2011), supporting a critical role for Hsps in proper

481 neurodevelopment.

482 At the subcellular level, Hsc70 (Hsp70 family chaperone) and Hsp90 are localized to
483 the apical dendrites of Purkinje cells and cerebellar neurons from postnatal period into
484 adulthood (D'Souza and Brown, 1998); in the differentiating hippocampal neurons, Hsp90 was
485 associated with the cytoskeleton in branch points and terminal ends (Quinta and Galigniana,
486 2012). These results suggest that Hsps may regulate neuronal polarization and neurite
487 morphogenesis by modulating cytoskeleton dynamics. Indeed, pharmacological inhibition of
488 Hsp90 disturbed the polarization and axonal extension of cultured hippocampal neurons by
489 inhibiting the PI3K/Akt/GSK3 signaling pathway (Benitez et al., 2014), which is known to
490 regulate neuronal morphogenesis (Kim et al., 2011). The fact that Akt and GSK3 are Hsp90
491 client proteins (Banz et al., 2009; Sato et al., 2000) indicates that Hsp90 could regulate cell
492 differentiation by maintaining the stability of its client proteins. Thus, given that Hsp90
493 interacts with hundreds of client proteins, the specific function of Hsp90 in differentiation
494 would depend on the function of its client protein(s) in particular cellular contexts.

495 Our studies identified one such context, in which Hsp70/Hsp90 chaperones play an
496 unexpected, inhibitory role in regulating MT stability and neurite growth. In *mec-15(-)* mutants,
497 Hsp70/Hsp90 chaperone and co-chaperones contribute to destabilizing MTs, inhibiting neurite
498 growth, suppressing synaptic development, and disrupting sensory functions. Components of
499 this molecular chaperone machinery include HSP-110/Hsp70, HSP-90/Hsp90, cochaperone
500 STI-1/STI1/Hop (which links Hsp70 and Hsp90), PPH-5/PP5 (which interacts with and
501 activates Hsp90 and other cochaperones through dephosphorylation), DAF-41/p23/PTGES3
502 (which binds to Hsp90 in its ATP-bound conformation and stabilizes the Hsp90-substrate
503 complexes), and CDC-37/Cdc37 (which interacts with Hsp90 and promote the maturation of
504 kinase substrate) (Figure 7). Removing any of these components in *mec-15(-)* mutants rescued
505 the TRN developmental defects and restore normal differentiation. The fact that our
506 experiments identified almost every component in a Hsp90 ATPase cycle (or protein folding
507 cycle) suggests that a complete Hsp90 pathway is involved in negatively regulating TRN
508 differentiation.

509 At least part of this negative regulation is mediated by the stabilization of DLK-1,
510 which is a conserved Hsp90 client protein in *C. elegans* (this study), Drosophila, and mice

511 (Karney-Grobe et al., 2018). Because the loss of Hsp90 cochaperones fully rescued all
512 developmental defects in *mec-15(-)* mutants, whereas mutations in *dlk-1* only partially
513 suppressed the neurite growth defects, other client proteins stabilized by Hsp90 chaperones
514 may also participate in the inhibition of TRN differentiation. Future studies will focus on
515 identifying such clients.

516 **The opposing effects of UPS and chaperones in neuronal differentiation**

517 Mutations in the chaperones and cochaperones by themselves did not produce any
518 defects in TRN differentiation, suggesting that the inhibitory function of Hsp70/Hsp90
519 chaperones and cochaperones does not seem to affect normal development. This lack of effect
520 may be due to Hsp90 clients, such as DLK-1, being normally maintained at a low level by the
521 UPS involving MEC-15, making the effects of chaperone loss difficult to detect. In *mec-15(-)*
522 mutants, when DLK-1 and likely other Hsp90 client proteins accumulate in the TRNs, they are
523 stabilized by the Hsp70/Hsp90 chaperone machinery and exert their functions. In such
524 scenarios, the activity of chaperones in controlling differentiation becomes critical. Thus, by
525 targeting the Hsp90 clients for degradation, UPS curbs the activity of the chaperones in
526 inhibiting cellular differentiation.

527 These opposing effects of UPS and the chaperones are quite unexpected, since most
528 previous studies indicate that they work synergistically to degrade misfolded proteins. This
529 protein quality control safeguards axon guidance in developing neurons (Wang et al., 2013)
530 and prevents protein aggregation that leads to neurodegeneration (Ciechanover and Kwon,
531 2017). Our studies, however, provide novel insights into the interaction between UPS and
532 chaperones by suggesting that chaperones also promote the expression and stabilization of
533 proteins that are normally degraded by UPS for fast turnover and low background abundance.
534 This tug-of-war keeps the common substrate of UPS and chaperones at the optimal level, which
535 is crucial for a range of neurodevelopmental processes, including MT formation, neurite
536 growth, synaptic development, and neuronal functions, not only in the TRNs but also in the
537 GABAergic motor neurons. Therefore, we suspect that the balance between the UPS and
538 chaperone activities may be generally important for robust neuronal differentiation.

539

540

541 **Materials and Methods**

542 **Strains and Forward Genetic Screens**

543 *Caenorhabditis elegans* wild-type (N2) and mutant strains were maintained at 20°C
544 as previously described (Brenner, 1974). Alleles used in this study are described in the main
545 text. Most strains were provided by the Caenorhabditis Genetics Center, which is funded by
546 NIH Office of Research Infrastructure Programs (P40 OD010440) or the National BioResource
547 Project of Japan.

548 For the *mec-7(neo)* suppressor screen, we used TU4879 [*mec-7(u278) X; uIs115 (mec-*
549 *17p::TagRFP) IV*] as the starter strain, which showed the growth of a long ALM-PN, and ethyl
550 methanesulfonate (EMS) as the mutagen (Brenner, 1974). We isolated 30 mutants that showed
551 very short or no ALM-PN and outcrossed the mutants against TU4879 and identified the
552 phenotype-causing mutations through a combination of whole-genome resequencing,
553 candidate gene sequencing, and complementation tests. *mec-15(u1042)* was isolated from this
554 screen; details about other suppressors will be reported elsewhere.

555 For the *mec-15(-)* suppressor screen, we used TU5183 [*mec-15(u1042); mec-7(u278);*
556 *uIs115*] as the starter strain, which had a short or no ALM-PN, and EMS as the mutagen.
557 Through a screen of 29,153 haploid genomes, we isolated 12 mutants that had a prominent
558 ALM-PN with at least five cell body length and identified the phenotype-causing mutations in
559 8 of the mutants through whole-genome resequencing (Table S1). Deletion alleles *sti-1(ok3354)*
560 and *pph-5(ok3498)* and frameshift-causing allele *dlk-1(ju476)* were used as the reference
561 alleles.

562 **Candidate RNAi Screen**

563 To test Skp and Cullin homologs for the suppression of *mec-7(u278)*, we constructed
564 TU6023 *[eri-1(mg366ts) uIs115 IV; mec-7(u278) lin-15b(n744) X]* for enhanced RNAi effects
565 and performed feeding RNAi using bacteria colonies from the Ahringer library (Fraser et al.,
566 2000). Briefly, we seeded bacteria expressing dsRNA on NGM agar plates containing 6 mM
567 IPTG and 100 μg/ml ampicillin. One day later, eggs from TU6023 animals were placed onto
568 these plates, hatched, and grown to adults at 20°C. The F1 progeny of these worms were
569 examined for the growth of ALM-PN at the day one adult stage. Genes whose knockdown
570 shortened the ALM-PN length to below five cell body lengths were regarded as positive.

571 To test candidate genes for the suppression of *mec-15(-)* mutation, we constructed
572 TU6092 *[mec-15(u75); eri-1(mg366) uIs115; mec-7(u278) lin-15B(n744)]* and performed
573 feeding RNAi for the genes indicated in Table S2. Genes whose knockdown restored the ALM-
574 PN length to above five cell body lengths were regarded as positive; positives from the screen
575 were confirmed using deletion alleles, including *hsp-90(ok1333)*, *hsp-110(gk533)*, and *daf-*
576 *41(ok3052)*.

577 **Constructs and transgenes**

578 For *mec-15* reporter and expression constructs, a *mec-15::GFP* translational reporter
579 (TU#2278) was made by cloning a 3.2 kb promoter upstream of the translational start and the
580 entire *mec-15* coding sequence into the pPD95.75 backbone and was used to generate an
581 integrated transgene *unkIs1[mec-15::GFP]*. *mec-18p::mec-15* (TU#891) was generated
582 previously by inserting a 0.5-kb *mec-18* promoter and the *mec-15* coding sequence with a 1.6
583 kb 3'UTR into the pBlueScript II backbone (Bounoutas et al., 2009b). *mec-18p::mec-15(Δ9-*
584 *50)* (TU#2100), *mec-18p::mec-15(Δ9-84)* (TU#2101), and *mec-18p::mec-15::HA* (CGZ#84)
585 were generated via site-directed mutagenesis using TU#891 as a template.

586 For *pph-5* and *sti-1* reporter and expression constructs, the *pph-5* transcriptional
587 reporter transgene *avIs90[pph-5p::mCherry::H2B::pph-5 3'UTR; unc-119(+)]* was generated
588 by Richie et al. (2011). For the *pph-5* translational reporter, we amplified a 2.3-kb promoter,
589 the cDNA of *pph-5* (isoform a), and a 481-bp *pph-5* 3'UTR and assembled the PCR products
590 with amplified pUC57 backbone via HiFi assembly (New England Biolabs) to generate the
591 vector *pph-5p::pph-5(cDNA)::pph-5 3'UTR* (TU#2257). The GFP coding sequence was then
592 subcloned from pPD95.75 and inserted before the stop codon of *pph-5* to generate *pph-*
593 *5p::pph-5(cDNA)::GFP::pph-5 3'UTR* (TU#2267) via HiFi assembly. The *sti-1p::GFP::unc-*
594 *54 3'UTR* (TU#2202) transcriptional reporter was generated through the Gateway system (Life
595 Technologies) by cloning a 1045-bp promoter into pDONR-P4-P1r and then performing LR
596 reactions with pENTR-GFP, pENTR-unc-54-3' UTR, and destination vector pDEST-R4-R3.
597 We then generated *sti-1p::sti-1::sti-1 3'UTR* vector (TU#2264) by amplifying the backbone
598 plus the *sti-1* promoter from TU#2202 and the *sti-1* genomic coding sequence plus a 607-bp
599 3'UTR from genomic DNA and assembled them via HiFi assembly. GFP-coding sequence was
600 then inserted before the *sti-1* stop codon to generate *sti-1p::sti-1::GFP::sti-1 3'UTR*

601 (TU#2280).

602 For TRN-specific expression or RNAi constructs, *mec-17p::pph-5(cDNA)::pph-5*
603 *3'UTR* (TU#2266) was generated by swapping the *pph-5* promoter in TU# 2257 with a 2.9-kb
604 *mec-17* promoter. *mec-17p::sti-1::unc-54 3'UTR* (TU#2166), *mec-17p::daf-41::FLAG::unc-*
605 *54 3'UTR* (CGZ#92), *mec-17p::FLAG::dlk-1a::unc-54 3'UTR* (CGZ#78) were generated by
606 cloning *mec-17* promoter and *sti-1*, *daf-41*, and *dlk-1a* genomic coding sequences into the
607 Gateway vectors and then performing the LR reactions with pENTR-unc-54-3' UTR and
608 pDEST-R4-R3. GFP was inserted into CGZ#78 after the start codon of *dlk-1* to make *mec-*
609 *17p::GFP::dlk-1a::unc-54 3'UTR* (CGZ#71). Various *mec-17p::sti-1* mutant constructs were
610 generated by site-directed mutagenesis using TU#2166 as a template. For TRN-specific RNAi
611 of *uba-1*, *hsf-1*, and *cdc-37*, we amplified the sense and antisense sequences of their genomic
612 coding region (without start and stop codons), and inserted them downstream of a *mec-17*
613 promoter in pDEST-R4-R3 backbones; the resulting constructs *mec-17p::uba-1-sense*
614 (TU#2286), *mec-17p::uba-1-antisense* (TU#2287), *mec-17p::hsf-1-sense* (CGZ#97), *mec-*
615 *17p::hsf-1-antisense* (CGZ#98), *mec-17p::cdc-37-sense* (CGZ#82), and *mec-17p::cdc-37-*
616 *antisense* (CGZ#83) were injected in pairs into *mec-7(u278)* or *mec-15; mec-7* animals for
617 RNA interference. As negative controls for RNAi, we injected *mec-17p::gfp-sense* (CGZ#167)
618 and *mec-17p::gfp-antisense* (CGZ#168) into corresponding animals to express dsRNA against
619 GFP.

620 To generate transgenic animals, we injected DNA constructs (5 ng/μl for each
621 expression vector) into the animals to establish stable lines carrying an extrachromosomal array;
622 at least three independent lines were tested. In some cases, we integrated the arrays into the
623 genome through standard γ-irradiation (Mello and Fire, 1995) to generate integrated transgenes,
624 including *unkIs1[mec-15::GFP]* and *unkIs2[mec-17p::GFP::dlk-1]*. Those integrated lines
625 were outcrossed for at least 5 times before being examined.

626 Transgenes *uIs31[mec-17p::GFP] III*, *uIs115[mec-17p::RFP] IV*, and *uIs134[mec-*
627 *17p::RFP] V* were used to visualize TRN morphology (Zheng et al., 2015). *jsIs821[mec-*
628 *7p::GFP::RAB-3]* was used to assess synaptic vesicle localization (Bounoutas et al., 2009b).
629 *sEx10796[daf-41p::GFP]* was used to examine *daf-41* expression pattern. *juIs1[unc-*
630 *25p::SNB-1-GFP]* was used to examine synaptic puncta in the GABAergic motor neurons.

631 **Electron microscopy**

632 We fixed TU4065 [*uIs115(mec-17p::TagRFP)*], TU5598 [*mec-15(u1042); uIs115*],
633 TU5579 [*pph-5(ok3498); mec-15(u1042); uIs115*], and TU5580 [*sti-1(ok3354); mec-*
634 *15(u1042); uIs115*] adults grown at 20°C using either a chemical immersion (Hall, 1995) or a
635 modified high-pressure freezing/freeze substitution (HPF/FS) protocol (Zheng et al., 2017).
636 Chemical immersion was performed using 1% glutaraldehyde + 1% tannic acid in 0.1 M
637 phosphate buffer (pH7.0); and HPF/FS was done by a first fixation in 0.5% glutaraldehyde +
638 0.2% tannic acid at -90°C for 90 hours and then at -60°C for 4 hours, followed by a second
639 fixation in 2% osmium tetroxide + 0.2% uranyl acetate at -60°C for 16 hours and then at -30°C
640 for 16 hours.

641 Eighty-nanometer transverse sections were collected at multiple positions along both
642 the ALM anterior neurite and the PLM anterior neurites and poststained with uranium acetate
643 and lead citrate. JEOL JEM-1400Plus TEM with a Galan Orius SC1000B bottom-mount digital
644 camera or a Philips CM10 electron microscope with an attached Morada digital camera
645 (Olympus) was used to acquire the images. For each strain, we examined sections from at least
646 ten animals. For each animal, we collected sections from at least five different positions along
647 the neurite and counted the number of MTs in a cross-section, measured the MT diameter, and
648 counted the number of protofilaments in individual MTs, of which clear substructure were
649 observed. Data from ALML and ALMR were combined and PLML and PLMR combined.
650 Number of data points for each measurement is indicated in Figure 4B and 4D.

651 **Yeast two-hybrid assay and western blot**

652 Yeast media and plates were prepared according to recipes from Clontech and yeasts
653 were grown at 30°C. The yeast strain PJ69-4a used for the two-hybrid assays contains GAL1-
654 HIS3, GAL2-ADE2 and GAL7-lacZ reporters (Zheng et al., 2018). Vectors pGAD424 and
655 pGBT9 (Clontech) were used to express proteins fused to the yeast-activating domain (AD)
656 and -binding domain (BD), respectively. cDNA fragments of *mec-15*, *skr-1*, *hsp-90*, and *dlk-*
657 *1a* were cloned into the two-hybrid vectors using HiFi Assembly (NEB).

658 Combinations of the AD or BD vectors were co-transformed into yeast using the
659 Frozen-EZ II kit from Zymo Research and using empty vectors as negative controls. Growth
660 assays were performed by growing individual colonies overnight in selective media lacking

661 tryptophan and leucine and then diluting the cultures to OD600 = 0.5; a series of further 1:10
662 dilutions were made, and 10 µl of the diluted culture were spotted onto plates lacking histidine
663 to test the expression of the HIS3 reporter. Plates were imaged after 2 days of growth.

664 For western blot, transgenic animals were collected and lysed with the RIPA buffer
665 [25 mM Tris-HCl, pH 7.5; 100 mM NaCl, 1 mM EDTA, 0.5% NP-40, and freshly added
666 protease inhibitors] and sonicated for 15 cycles of 1 second on and 15 seconds off. The protein
667 lysate was then separated by SDS-PAGE and blotted with anti-HA (Cat# HT301-02, TransGen
668 Biotech, Beijing) and anti-FLAG (Cat# F1804, Sigma) primary antibodies and HRP-
669 conjugated secondary antibodies (Cat# A9044, Sigma).

670 **Fluorescent imaging, aldicarb assay, phenotype scoring and statistical analysis**

671 Fluorescent imaging was done either on a Zeiss Axio Observer Z1 inverted
672 microscope equipped with a CoolSNAP HQ2-FW camera (Photometrics) or a Leica DMi8
673 inverted microscope equipped with a Leica DFC7000 GT monochrome camera. Measurements
674 were made using either the Zeiss AxioVision (SE64 Rel. 4.9.1) or the Leica Application Suite
675 X (3.7.0.20979) software.

676 We measured the length of TRN neurites in at least 20 larvae or young adults grown
677 at 20°C, except where otherwise stated. Normalized neurite length was calculated by dividing
678 the neurite length by the diameter of the cell body along A-P axis. Defects in PLM-AN growth
679 were assessed by measuring the distance from the PLM-AN terminals to the center of the vulva.
680 Positive numbers mean PLM-AN terminals are more anterior than the vulva; negative numbers
681 mean PLM-AN did not reach the vulva; at least 30 cells were examined for each strain. All bar
682 graphs show mean ± SD.

683 Fluorescence intensity of the TagRFP expressed from the *uIs115[mec-17p::TagRFP]*
684 or the GFP expression from *unkIs2[mec-17p::GFP::dlk-1]* transgene in the PLM cell body was
685 used to measure TRN protein levels; intensity was measured by first acquiring images using
686 the identical exposure time and laser power and then manually subtracting the background from
687 the fluorescent signal using ImageJ. At least 30 cells were imaged and analyzed for each strain.

688 For the assay of sensitivity to aldicarb, an acetylcholinesterase inhibitor, 20 day-one
689 adult animals were transferred onto NGM plates containing 1 mM aldicarb (Sigma) without
690 food. The number of animals that were paralyzed was recorded every 10 minutes, starting at

30 minutes after the transfer. Genotypes were blind to the experimenter, and the assay was repeated three times.

For statistical analysis, analysis of variance and the post hoc Dunnett's test (comparison of each of many treatments with a single control) or Tukey–Kramer test (studentized range test for all pair-wise comparison) were performed using the GraphPad Prism (version 8.00 for Mac, GraphPad Software, La Jolla, CA; www.graphpad.com) to identify significant difference among samples. Student's t test was used to find significant difference between two samples in paired comparisons. Single and double asterisks indicate $p < 0.05$ and $p < 0.01$, respectively.

Acknowledgements

We thank Natalie Yvonne Sayegh for helping with the *mec-7* suppressor screen, Andy Golden for sharing strains carrying *avIs90*, and the members of the Chalfie lab for constructive comments on the manuscript. This work is supported by start-up funds from the University of Hong Kong to C.Z. and grants from the Research Grant Council of Hong Kong [ECS27104219 to C.Z.] and the National Institutes of Health of United States [GM30997 and GM122522 to M.C.; OD010943 to D.H.H.]. The electron microscope JEOL 1400Plus TEM used in this study was acquired through a NIH Shared Instrumentation Grant (1S10OD016214-01A1) at Albert Einstein College of Medicine.

Competing interests

The authors declare no competing or financial interests.

Author Contributions

Conceptualization, C.Z. and M.C.; Methodology, C.Z., E.A., K.C.Q.N, D.H.H., and M.C.; Investigation, C.Z., E.A., H.M.T.L, S.L.J.J, and K.C.Q.N; Writing – Original draft and revision, C.Z. and M.C.; Funding acquisition, C.Z., D.H.H., and M.C.; Resource, D.H.H.; Supervision, C.Z. and M.C.

721 # Reference

722 **Banz, V. M., Medova, M., Keogh, A., Furer, C., Zimmer, Y., Candinas, D. and Stroka, D.** (2009). Hsp90
723 transcriptionally and post-translationally regulates the expression of NDRG1 and maintains the stability
724 of its modifying kinase GSK3beta. *Biochim Biophys Acta* **1793**, 1597-1603.

725 **Benitez, M. J., Sanchez-Ponce, D., Garrido, J. J. and Wandosell, F.** (2014). Hsp90 activity is necessary to acquire
726 a proper neuronal polarization. *Biochim Biophys Acta* **1843**, 245-252.

727 **Bounoutas, A., Kratz, J., Emtage, L., Ma, C., Nguyen, K. C. and Chalfie, M.** (2011). Microtubule depolymerization
728 in Caenorhabditis elegans touch receptor neurons reduces gene expression through a p38 MAPK
729 pathway. *Proc Natl Acad Sci U S A* **108**, 3982-3987.

730 **Bounoutas, A., O'Hagan, R. and Chalfie, M.** (2009a). The multipurpose 15-protofilament microtubules in C.
731 elegans have specific roles in mechanosensation. *Curr Biol* **19**, 1362-1367.

732 **Bounoutas, A., Zheng, Q., Nonet, M. L. and Chalfie, M.** (2009b). mec-15 encodes an F-box protein required for
733 touch receptor neuron mechanosensation, synapse formation and development. *Genetics* **183**, 607-617,
734 601SI-604SI.

735 **Brenner, S.** (1974). The genetics of Caenorhabditis elegans. *Genetics* **77**, 71-94.

736 **Buchberger, A., Bukau, B. and Sommer, T.** (2010). Protein quality control in the cytosol and the endoplasmic
737 reticulum: brothers in arms. *Mol Cell* **40**, 238-252.

738 **Chalfie, M. and Au, M.** (1989). Genetic control of differentiation of the Caenorhabditis elegans touch receptor
739 neurons. *Science* **243**, 1027-1033.

740 **Cheng, P. L., Lu, H., Shelly, M., Gao, H. and Poo, M. M.** (2011). Phosphorylation of E3 ligase Smurf1 switches its
741 substrate preference in support of axon development. *Neuron* **69**, 231-243.

742 **Ciechanover, A. and Kwon, Y. T.** (2017). Protein Quality Control by Molecular Chaperones in Neurodegeneration.
743 *Front Neurosci* **11**, 185.

744 **D'Souza, S. M. and Brown, I. R.** (1998). Constitutive expression of heat shock proteins Hsp90, Hsc70, Hsp70 and
745 Hsp60 in neural and non-neural tissues of the rat during postnatal development. *Cell Stress Chaperones*
746 **3**, 188-199.

747 **Fraser, A. G., Kamath, R. S., Zipperlen, P., Martinez-Campos, M., Sohrmann, M. and Ahringer, J.** (2000).
748 Functional genomic analysis of C. elegans chromosome I by systematic RNA interference. *Nature* **408**,
749 325-330.

750 **Gillan, V., Maitland, K., McCormack, G., Him, N. A. and Devaney, E.** (2009). Functional genomics of hsp-90 in
751 parasitic and free-living nematodes. *Int J Parasitol* **39**, 1071-1081.

752 **Hall, D. H.** (1995). Electron microscopy and three-dimensional image reconstruction. *Methods Cell Biol* **48**, 395-
753 436.

754 **Hartl, F. U., Bracher, A. and Hayer-Hartl, M.** (2011). Molecular chaperones in protein folding and proteostasis.
755 *Nature* **475**, 324-332.

756 **Hsu, J. M., Chen, C. H., Chen, Y. C., McDonald, K. L., Gurling, M., Lee, A., Garriga, G. and Pan, C. L.** (2014).
757 Genetic analysis of a novel tubulin mutation that redirects synaptic vesicle targeting and causes neurite
758 degeneration in C. elegans. *PLoS Genet* **10**, e1004715.

759 **Ishimoto, T., Kamei, A., Koyanagi, S., Nishide, N., Uyeda, A., Kasai, M. and Taguchi, T.** (1998). HSP90 has neurite-
760 promoting activity in vitro for telencephalic and spinal neurons of chick embryos. *Biochem Biophys Res*
761 *Commun* **253**, 283-287.

762 **Karney-Grobe, S., Russo, A., Frey, E., Milbrandt, J. and DiAntonio, A.** (2018). HSP90 is a chaperone for DLK and
763 is required for axon injury signaling. *Proc Natl Acad Sci U S A* **115**, E9899-E9908.

764 **Kim, Y. T., Hur, E. M., Snider, W. D. and Zhou, F. Q.** (2011). Role of GSK3 Signaling in Neuronal Morphogenesis.

765 *Front Mol Neurosci* **4**, 48.
766 **Konishi, Y., Stegmuller, J., Matsuda, T., Bonni, S. and Bonni, A.** (2004). Cdh1-APC controls axonal growth and
767 patterning in the mammalian brain. *Science* **303**, 1026-1030.
768 **Lindquist, S. and Craig, E. A.** (1988). The heat-shock proteins. *Annu Rev Genet* **22**, 631-677.
769 **Loones, M. T., Chang, Y. and Morange, M.** (2000). The distribution of heat shock proteins in the nervous system
770 of the unstressed mouse embryo suggests a role in neuronal and non-neuronal differentiation. *Cell*
771 *Stress Chaperones* **5**, 291-305.
772 **Mello, C. and Fire, A.** (1995). DNA transformation. *Methods Cell Biol* **48**, 451-482.
773 **Miller, D. J. and Fort, P. E.** (2018). Heat Shock Proteins Regulatory Role in Neurodevelopment. *Front Neurosci* **12**,
774 821.
775 **Nakata, K., Abrams, B., Grill, B., Goncharov, A., Huang, X., Chisholm, A. D. and Jin, Y.** (2005). Regulation of a
776 DLK-1 and p38 MAP kinase pathway by the ubiquitin ligase RPM-1 is required for presynaptic
777 development. *Cell* **120**, 407-420.
778 **Quinta, H. R. and Galigniana, M. D.** (2012). The neuroregenerative mechanism mediated by the Hsp90-binding
779 immunophilin FKBP52 resembles the early steps of neuronal differentiation. *Br J Pharmacol* **166**, 637-
780 649.
781 **Richie, C. T., Bembenek, J. N., Chestnut, B., Furuta, T., Schumacher, J. M., Wallenfang, M. and Golden, A.** (2011).
782 Protein phosphatase 5 is a negative regulator of separase function during cortical granule exocytosis in
783 C. elegans. *J Cell Sci* **124**, 2903-2913.
784 **Rohl, A., Tippel, F., Bender, E., Schmid, A. B., Richter, K., Madl, T. and Buchner, J.** (2015). Hop/Sti1
785 phosphorylation inhibits its co-chaperone function. *EMBO Rep* **16**, 240-249.
786 **Sato, S., Fujita, N. and Tsuruo, T.** (2000). Modulation of Akt kinase activity by binding to Hsp90. *Proc Natl Acad*
787 *Sci U S A* **97**, 10832-10837.
788 **Schaefer, A. M., Hadwiger, G. D. and Nonet, M. L.** (2000). rpm-1, a conserved neuronal gene that regulates
789 targeting and synaptogenesis in C. elegans. *Neuron* **26**, 345-356.
790 **Schmid, A. B., Lagleder, S., Grawert, M. A., Rohl, A., Hagn, F., Wandinger, S. K., Cox, M. B., Demmer, O., Richter,**
791 **K., Groll, M., et al.** (2012). The architecture of functional modules in the Hsp90 co-chaperone Sti1/Hop.
792 *EMBO J* **31**, 1506-1517.
793 **Schwamborn, J. C., Muller, M., Becker, A. H. and Puschel, A. W.** (2007). Ubiquitination of the GTPase Rap1B by
794 the ubiquitin ligase Smurf2 is required for the establishment of neuronal polarity. *EMBO J* **26**, 1410-
795 1422.
796 **Singh, V. and Aballay, A.** (2006). Heat-shock transcription factor (HSF)-1 pathway required for Caenorhabditis
797 elegans immunity. *Proc Natl Acad Sci U S A* **103**, 13092-13097.
798 **Song, H. O., Lee, W., An, K., Lee, H. S., Cho, J. H., Park, Z. Y. and Ahnn, J.** (2009). C. elegans STI-1, the homolog
799 of Sti1/Hop, is involved in aging and stress response. *J Mol Biol* **390**, 604-617.
800 **Sun, Y., Hu, Z., Goeb, Y. and Dreier, L.** (2013). The F-box protein MEC-15 (FBXW9) promotes synaptic transmission
801 in GABAergic motor neurons in C. elegans. *PLoS One* **8**, e59132.
802 **Tang, N. H. and Chisholm, A. D.** (2016). Regulation of Microtubule Dynamics in Axon Regeneration: Insights from
803 C. elegans. *F1000Res* **5**.
804 **Tedeschi, A. and Bradke, F.** (2013). The DLK signalling pathway--a double-edged sword in neural development
805 and regeneration. *EMBO Rep* **14**, 605-614.
806 **Tuoc, T. C. and Stoykova, A.** (2010). Roles of the ubiquitin-proteosome system in neurogenesis. *Cell Cycle* **9**, 3174-
807 3180.
808 **Uchida, S., Hara, K., Kobayashi, A., Fujimoto, M., Otsuki, K., Yamagata, H., Hobara, T., Abe, N., Higuchi, F.,**

809 **Shibata, T., et al.** (2011). Impaired hippocampal spinogenesis and neurogenesis and altered affective
810 behavior in mice lacking heat shock factor 1. *Proc Natl Acad Sci U S A* **108**, 1681-1686.
811 **Vaughan, C. K., Mollapour, M., Smith, J. R., Truman, A., Hu, B., Good, V. M., Panaretou, B., Neckers, L., Clarke,**
812 **P. A., Workman, P., et al.** (2008). Hsp90-dependent activation of protein kinases is regulated by
813 chaperone-targeted dephosphorylation of Cdc37. *Mol Cell* **31**, 886-895.
814 **Wandinger, S. K., Suhre, M. H., Wegele, H. and Buchner, J.** (2006). The phosphatase Ppt1 is a dedicated regulator
815 of the molecular chaperone Hsp90. *EMBO J* **25**, 367-376.
816 **Wang, Z., Hou, Y., Guo, X., van der Voet, M., Boxem, M., Dixon, J. E., Chisholm, A. D. and Jin, Y.** (2013). The
817 EBAX-type Cullin-RING E3 ligase and Hsp90 guard the protein quality of the SAX-3/Robo receptor in
818 developing neurons. *Neuron* **79**, 903-916.
819 **Watkins, T. A., Wang, B., Huntwork-Rodriguez, S., Yang, J., Jiang, Z., Eastham-Anderson, J., Modrusan, Z.,**
820 **Kaminker, J. S., Tessier-Lavigne, M. and Lewcock, J. W.** (2013). DLK initiates a transcriptional program
821 that couples apoptotic and regenerative responses to axonal injury. *Proc Natl Acad Sci U S A* **110**, 4039-
822 4044.
823 **Wayne, N., Mishra, P. and Bolon, D. N.** (2011). Hsp90 and client protein maturation. *Methods Mol Biol* **787**, 33-
824 44.
825 **Yamada, T., Yang, Y. and Bonni, A.** (2013). Spatial organization of ubiquitin ligase pathways orchestrates neuronal
826 connectivity. *Trends Neurosci* **36**, 218-226.
827 **Yan, D. and Jin, Y.** (2012). Regulation of DLK-1 kinase activity by calcium-mediated dissociation from an inhibitory
828 isoform. *Neuron* **76**, 534-548.
829 **Yan, D., Wu, Z., Chisholm, A. D. and Jin, Y.** (2009). The DLK-1 kinase promotes mRNA stability and local translation
830 in C. elegans synapses and axon regeneration. *Cell* **138**, 1005-1018.
831 **Zheng, C., Diaz-Cuadros, M. and Chalfie, M.** (2015). Dishevelled attenuates the repelling activity of Wnt signaling
832 during neurite outgrowth in Caenorhabditis elegans. *Proc Natl Acad Sci U S A* **112**, 13243-13248.
833 **Zheng, C., Diaz-Cuadros, M., Nguyen, K. C. Q., Hall, D. H. and Chalfie, M.** (2017). Distinct effects of tubulin
834 isotype mutations on neurite growth in Caenorhabditis elegans. *Mol Biol Cell* **28**, 2786-2801.
835 **Zheng, C., Jin, F. Q., Trippe, B. L., Wu, J. and Chalfie, M.** (2018). Inhibition of cell fate repressors secures the
836 differentiation of the touch receptor neurons of Caenorhabditis elegans. *Development* **145**.
837
838
839
840
841
842
843
844
845
846
847

848 **Figure legends:**

849 **Figure 1. F-box protein MEC-15 promotes neurite growth.** (A) The ALM-PN is missing in the wild
850 type animals (arrow head) but is extensive (arrow) in *mec-7(u278 neo)* mutants. *mec-15 lf* mutations
851 suppressed ALM-PN production in *mec-7(u278)* mutants, but the ALM-PN can be restored in the
852 double mutants by expressing wild-type MEC-15 under a TRN-specific *mec-18* promoter. (B)
853 Schematic presentation of ALM and PLM morphologies (with labelled neurites) in wild-type and
854 mutant animals. (C) Protein structures of the wild-type MEC-15 with the F-Box and the four WD-40
855 repeats (WD) labeled in green and blue, respectively. (D) The normalized length (mean ± SD) of ALM-
856 PN in various strains. Here and in all the other Figures, error bars represent standard deviation, and
857 asterisks indicate significant difference (* for $p < 0.05$ and ** for $p < 0.01$) in ANOVA and Tukey-
858 Kramer test. (E) TRN morphology in *mec-15(u75 lf)* mutants. (i) low magnification view. (ii) PLM-AN
859 (arrow) was shortened and did not extend beyond PVM. (iii) PLM-PN (arrow) was also significantly
860 shortened. Synaptic branches (arrow) of (iv) ALM-AN and (v) PLM-AN could not fully extend in *mec-*
861 *15* mutants. (F) The expression of *mec-15::GFP* in (i) anterior and (ii) posterior TRNs, (iii) head
862 neurons, (iv) ventral cord neurons, and (v) the preanal ganglion and the tail.

863 **Figure 2. Loss of Hsp90 chaperones suppress the neurite growth defects in *mec-15 lf* mutants.** (A)
864 ALM-PN is absent in *mec-15; mec-7* mutants (arrow head) and restored in triple mutants *sti-1* and *pph-*
865 *5 lf* mutations (arrow). (B) Schematic presentation of ALM and PLM morphologies in wild type and
866 various mutants. *sti-1(-)* is used as an example of *mec-15(-)* suppressors. (C) The length of ALM-PN in
867 various mutants. *hsp-90(ok1333)*, *hsp-1(ok1371)*, and *hsp-110(gk533)* alleles caused larval arrest and
868 were examined at L2/L3 stages. *daf-41(ok3052)*, *sti-1(u1071)*, and *pph-5(u1072)* were examined at both
869 L2/L3 and adult stages; *sti-1(ok3354)* and *pph-5(ok3498)* deletion alleles served as references. *mec-15;*
870 *mec-7* adult animals carrying transgenes expressing dsRNA against *hsf-1* or *cdc-37* in TRNs were
871 examined; results are labeled as *hsf-1(i)* and *cdc-37(i)*, respectively. (D) Premature termination of ALM-
872 AN and PLM-AN (arrow heads) in *mec-15* single mutants were rescued in *mec-15; sti-1* and *mec-15;*
873 *pph-5* double mutants. Dashed line indicates the position of the vulva. (E) Shortening of PLM-PN
874 (arrow head) in *mec-15* single mutants were rescued to its normal length (arrows) in the double mutants.
875 (F) Anterior extent of PLM-AN growth in one-day old adults of various mutants grown at 25°C.
876 Distances are given relative to the position of the vulva, so positive values indicate that the PLM-AN
877 grew past the vulva towards the anterior. (G) PLM-PN length in wild type (WT) and various mutants.

878 For (F) and (G), *daf-41(ok3052)*, *sti-1(u1071)*, *pph-5(u1072)*, *hsp-1(ok1371)*, *hsp-90(ok1333)*, and *hsp-*
879 *110(gk533)* were examined. Asterisks indicate statistical significance for the difference between the
880 *mec-7; mec-15* and the triple mutants (C) or between *mec-15* and the double mutants (G) in ANOVA
881 and Tukey-Kramer test.

882 **Figure 3. Phosphorylation inhibits STI-1 activity.** (A) Schematic representation of domain structure
883 of *C. elegans* STI-1 and its yeast and human homologs. Potential phosphorylation sites for *C. elegans*
884 STI-1 are shown. (B-D) The length of ALM-PN in *mec-7; mec-15; pph-5* triple mutants or *mec-7* single
885 mutants or *mec-7; mec-15* double mutants in the absence of *sti-1* transgene (-) or in the presence of the
886 wild type (WT) or the mutant STI-1 proteins expressed from the *mec-17* promoter. Double asterisks
887 indicate statistical significance ($p < 0.01$) between the control and the test group in ANOVA and
888 Dunnett's tests.

889 **Figure 4. The loss of MTs and TRN developmental and functional defects in *mec-15* mutants were**
890 **rescued by mutations in Hsp90 cochaperones.** (A) Representative EM micrographs of cross-sections
891 of ALM-AN and PLM-AN in wild-type, *mec-15(u1042)*, *mec-15; pph-5(ok3498)*, and *mec-15; sti-*
892 *1(ok3354)* animals. Scale bar = 100 nm. (B) Average number of MTs in a cross-section of ALM-AN
893 and PLM-AN in various strains. Numbers of sections analyzed for each strain are indicated above the
894 bars. The sections are from at least ten animals. (C) Enlarged EM images of individual MTs with
895 protofilament visualized by tannic acid staining from the cross-sections of PLM-AN of the strains
896 shown in (A). (D) Average diameter of MTs in cross-sections from various strains. Number of MTs
897 measured are indicated above the bars. In (B) and (D), double asterisks indicate statistical significance
898 ($p < 0.01$) for the difference between *mec-15* mutants and the double mutants. (E) Fluorescent intensity
899 of TagRFP in PLM expressed from the *uIs115[mec-17p::TagRFP]* transgene in *mec-15(u1042)*, *mec-*
900 *15; pph-5(ok3498)*, *mec-15; sti-1(ok3354)*, and *mec-15; daf-41(ok3052)* mutants. Quantification is in
901 arbitrary units for comparison. Representative images are shown with fluorescence only and
902 fluorescence and DIC. (F) Localization of synaptic vesicles labeled by GFP::RAB-3 in TRNs of wild-
903 type, *mec-15*, *mec-15; sti-1*, and *mec-15; pph-5* animals. (G) The number of gentle touch responses
904 from five gentle touch sitmuli in the strains indicated at 20°C. Double asterisks indicate statistical
905 significance ($p < 0.01$) for the difference between *mec-15* mutants and the double mutants.

906 **Figure 5. DLK-1 acts downstream of the chaperones to destabilize MTs and inhibit neurite growth.**

907 (A) Gene structure of the long isoform (a) of *dlk-1* and the positions of three *lf* mutations. (B) Effects
908 of *dlk-1* mutations on the normalized neurite length of ALM-PN and PLM-PN in *mec-15(u1042); mec-*
909 *7(u278)* animals. The ALM-PN length in *ju476/+* animals was examined in male cross progeny. Double
910 asterisks indicate significant difference ($p < 0.01$) between the test group and *mec-15; mec-7* double
911 mutants. (C) The length of PLM-PN in *dlk-1; mec-15* mutants and wild-type animals expressing *mec-*
912 *17p::dlk-1a* transgene. (D) The distance between the PLM-AN terminal and the vulva in the *dlk-1; mec-*
913 *15* mutants grown at 25°C. (E) The length of ALM-PN in *mec-7(u278)* animals with indicated mutant
914 genotype. Some animals expressed a *mec-17p::dlk-1a* transgene. The *dlk-1(ju476)*, *sti-1(ok3354)*, and
915 *pph-5(ok3498)* alleles were used. (F) Yeast two-hybrid assays for the interaction between AD::HSP-90
916 and BD::DLK-1a. AD means the Gal4 activation domain and BD means the Gal4 DNA-binding domain.
917 (G) Fluorescent intensity of GFP::DLK-1 expressed from the TRN-specific *mec-17* promoter in wild
918 type, *sti-1(ok3354)*, *pph-5(ok3498)*, and *mec-15(u1042)* mutants and animals carrying *mec-17p::uba-*
919 *1RNAi* transgenes. Dashed circles enclose PLM cell bodies; scale bar = 20 μm. Double asterisks indicate
920 significant difference from WT. (H) Fluorescent intensity of TagRFP expressed from *mec-17* promoter
921 in *dlk-1; mec-15* double mutants and in wild type animals expressing *mec-17p::dlk-1a* transgene.

922 **Figure 6. MEC-15 regulates synaptic functions of GABAergic motor neuron by antagonizing the**
923 **activity of Hsp90 chaperones.** (A) Synaptic puncta in the ventral neurite of GABAergic motor neurons
924 labeled by *juIs1[unc-25p::snb-1::GFP]* in the wild-type animal, *mec-15*, *mec-15; sti-1*, and *mec-15;*
925 *pph-5* mutants. (B) Average fluorescent intensity (arbitrary unit; AU) of the SNB-1::GFP puncta in the
926 indicated strains. (C) Average number of SNB-1::GFP puncta in 10 μm of the ventral neurite of
927 GABAergic motor neurons in the indicated strains. (D) Percentage of adult animals paralyzed at the
928 indicated time point after being exposed to 1 mM Aldicarb. Animals were raised from embryos to young
929 adults at either 20°C or 25°C before test. 20 animals and three replicates were used in each experiment.
930 The experiment was repeated three times; mean ± SD was shown. The same *mec-15* data were plotted
931 twice in the two graphs for comparing with the double mutants.

932 **Figure 7. A model for the antagonism between the activities of Hsp70/Hsp90 chaperone machinery**
933 **and MEC-15 in the regulation of TRN differentiation and functions.** HSP-90 receives client protein
934 X from either HSP-110 (a Hsp70 family protein) via a STI-1-mediated physical link or CDC-37 via its
935 binding to kinase clients. Both STI-1 and CDC-37 are activated by PPH-5 through dephosphorylation

936 (dashed line). Those Hsp90 client proteins, including DLK-1 and other unidentified proteins (?), are not
937 only stabilized by the chaperones but also subjected to MEC-15-mediated ubiquitination and
938 degradation. The antagonism between the chaperones and MEC-15 tightly controls the levels of those
939 Hsp90 client proteins, which appear to negatively regulate MT stability, neurite growth, and synaptic
940 development.

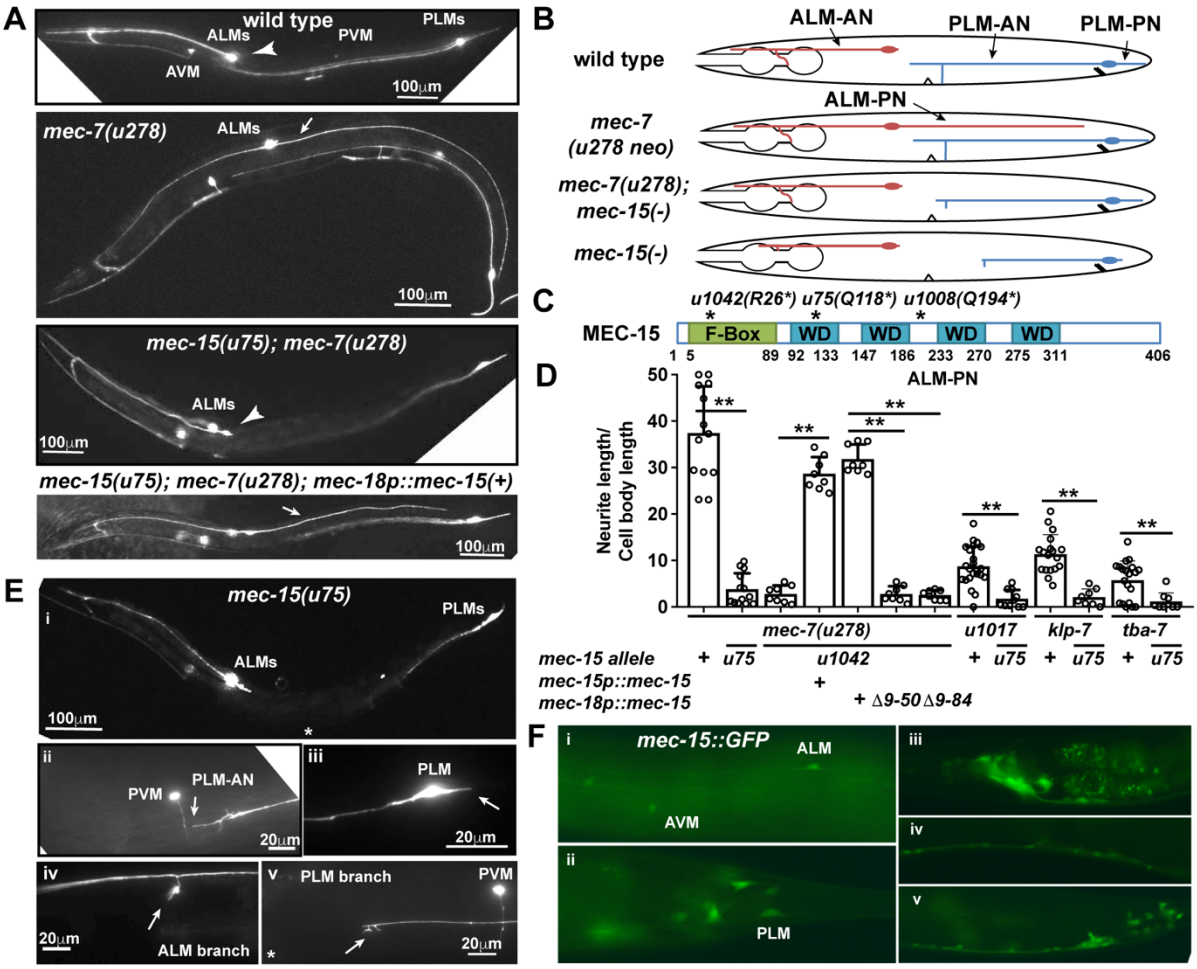
A
wild type
ALMs
PVM
PLMs
AVM
100µm
mec-7(u278)
ALMs
100µm
mec-15(u75); mec-7(u278)
ALMs
100µm
mec-15(u75); mec-7(u278); mec-18p::mec-15(+)
100µm
B
ALM-AN
PLM-AN
PLM-PN
wild type
ALM-PN
mec-7
(u278 neo)
mec-7(u278);
mec-15(-)
mec-15(-)
C
u1042(R26*) u75(Q118*) u1008(Q194*)
MEC-15
F-Box
WD
WD
WD
WD
1 5 89 92 133 147 186 233 270 275 311 406
D
ALM-PN
Neurite length/
Cell body length
mec-7(u278)
u1017
klp-7
tba-7
mec-15 allele
mec-15p::mec-15
mec-18p::mec-15
u75
u1042
Δ9-50Δ9-84
E
mec-15(u75)
PLMs
ALMs
100µm
PVM
PLM-AN
20µm
PLM
20µm
20µm
ALM branch
PLM branch
PVM
20µm
F
mec-15::GFP
ALM
AVM
PLM

Figure 1

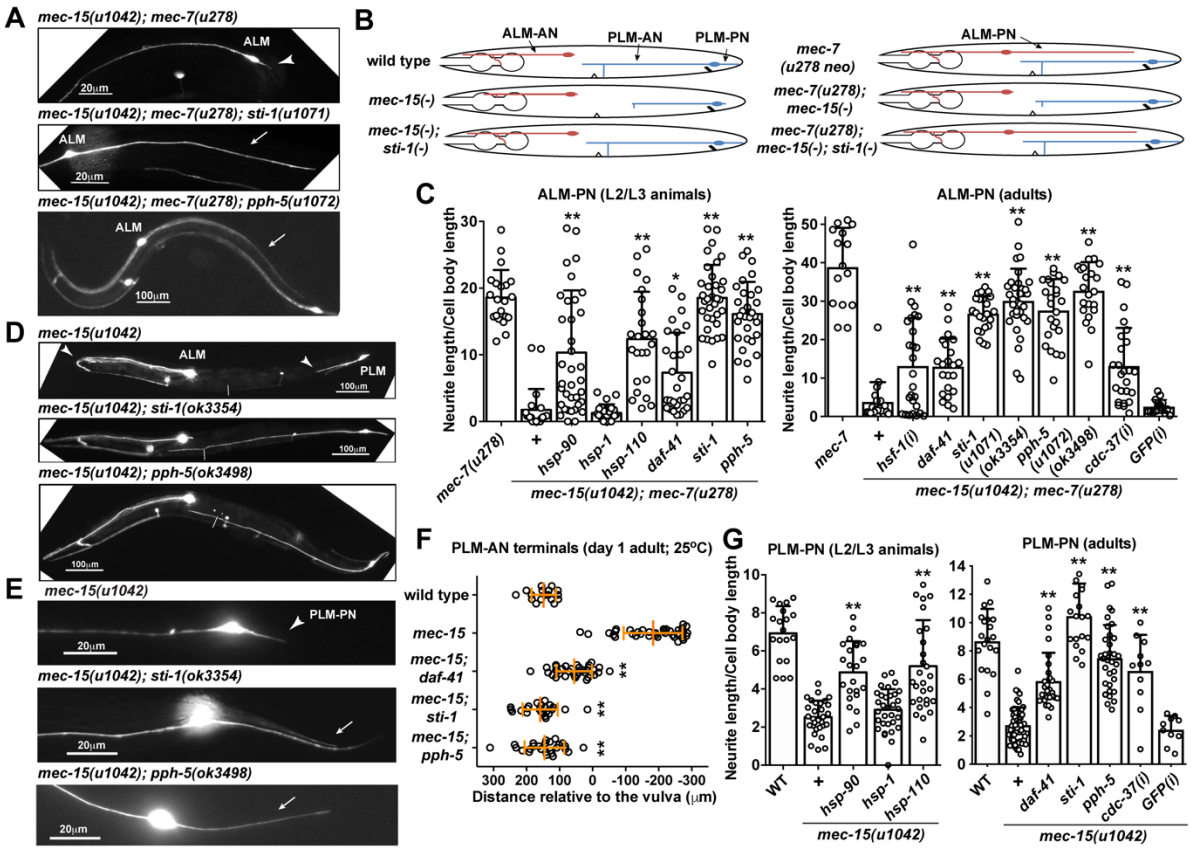

Figure 2

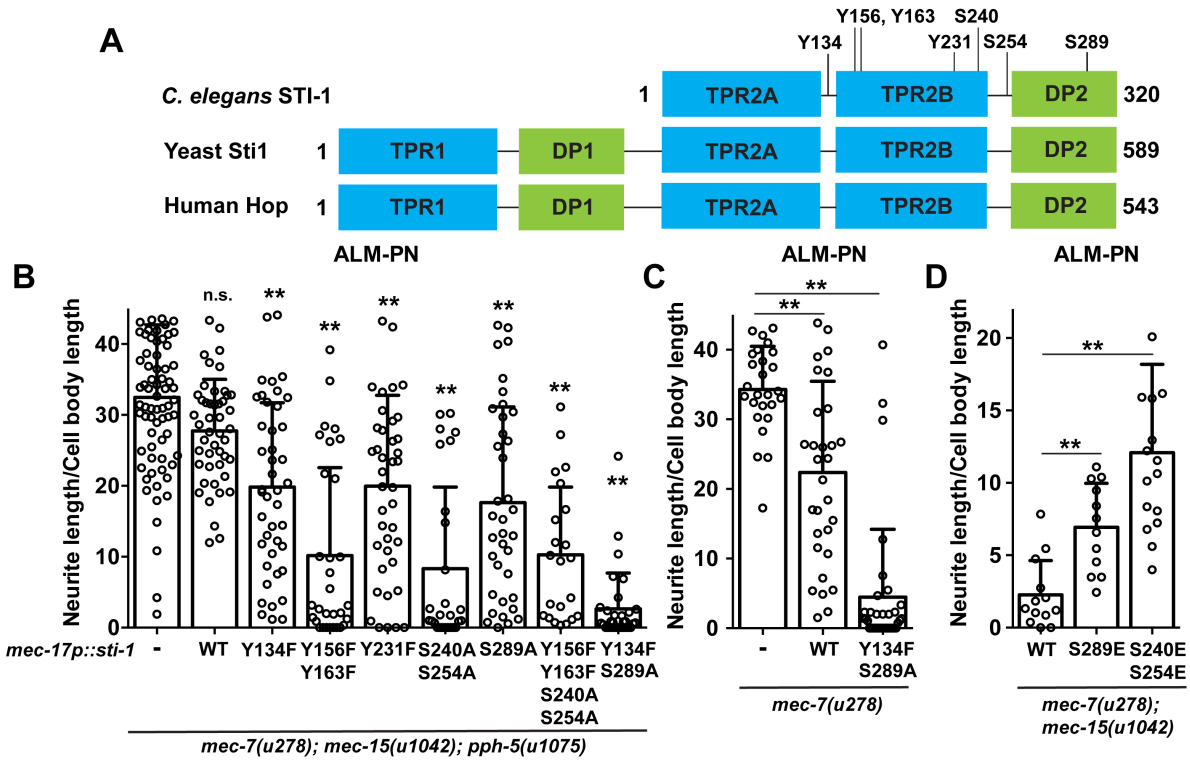

Figure 3

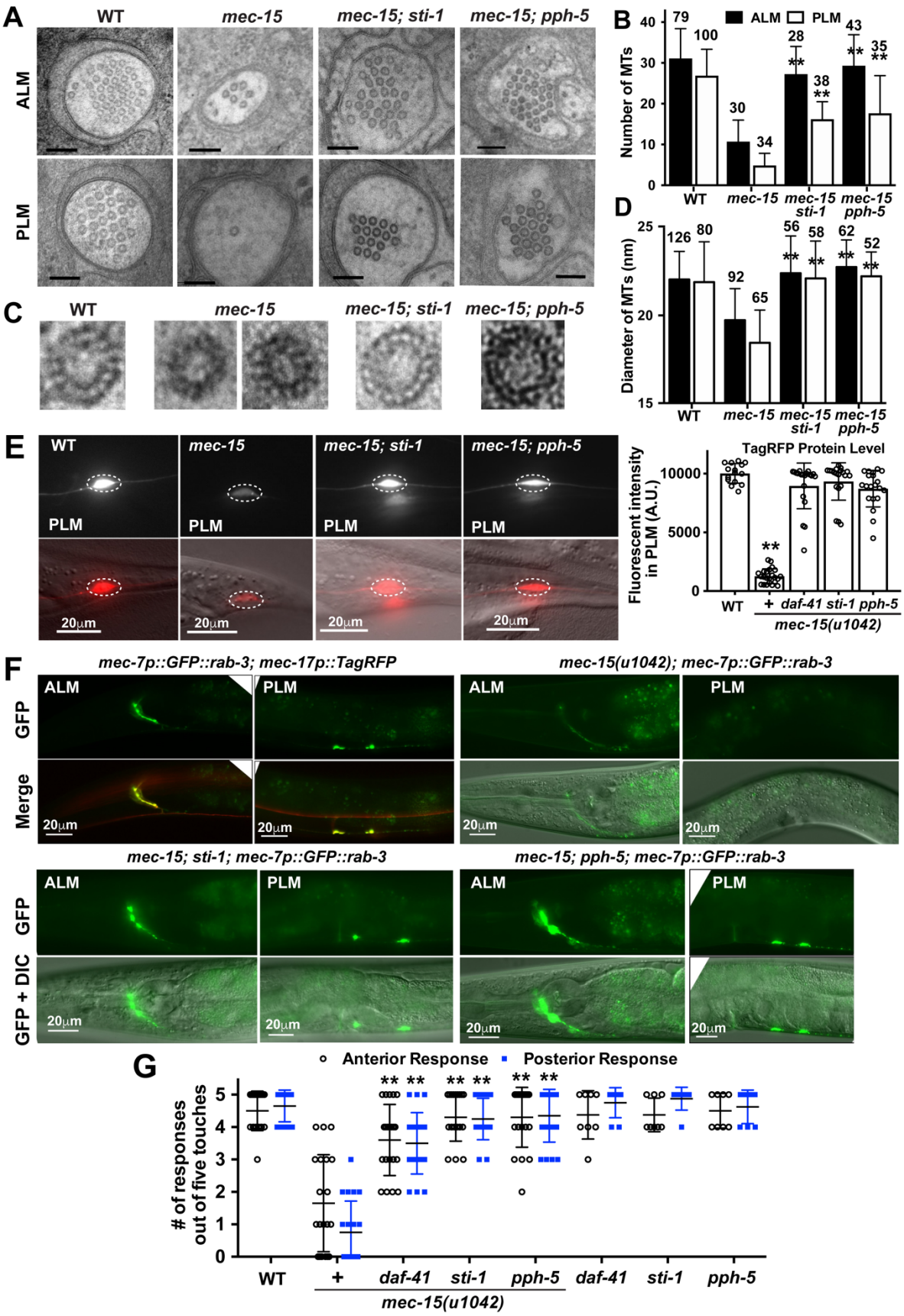
A
WT
mec-15
mec-15; sti-1
mec-15; pph-5
ALM
PLM
B
ALM
PLM
Number of MTs
79
100
30
34
28
38
43
35
WT
mec-15
mec-15 sti-1
mec-15 pph-5
C
WT
mec-15
mec-15; sti-1
mec-15; pph-5
D
Diameter of MTs (nm)
126
80
92
65
56
58
62
52
E
WT
mec-15
mec-15; sti-1
mec-15; pph-5
PLM
20μm
TagRFP Protein Level
Fluorescent intensity in PLM (A.U.)
10000
5000
0
WT
+
daf-41
sti-1
pph-5
mec-15(u1042)
F
mec-7p::GFP::rab-3; mec-17p::TagRFP
mec-15(u1042); mec-7p::GFP::rab-3
GFP
Merge
ALM
PLM
mec-15; sti-1; mec-7p::GFP::rab-3
mec-15; pph-5; mec-7p::GFP::rab-3
GFP + DIC
G
Anterior Response
Posterior Response
# of responses out of five touches
WT
+
daf-41
sti-1
pph-5
mec-15(u1042)

Figure 4

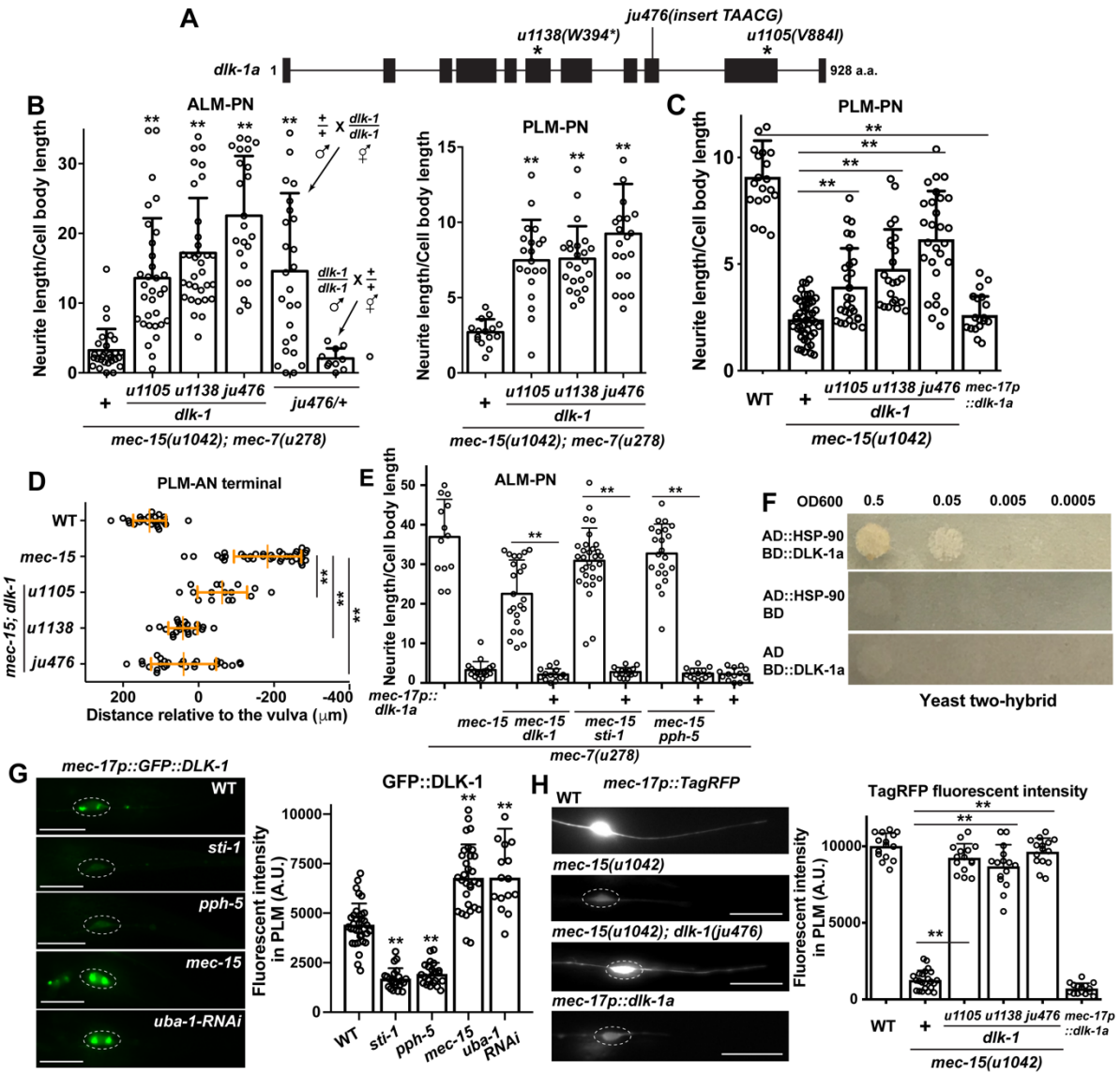

Figure 5

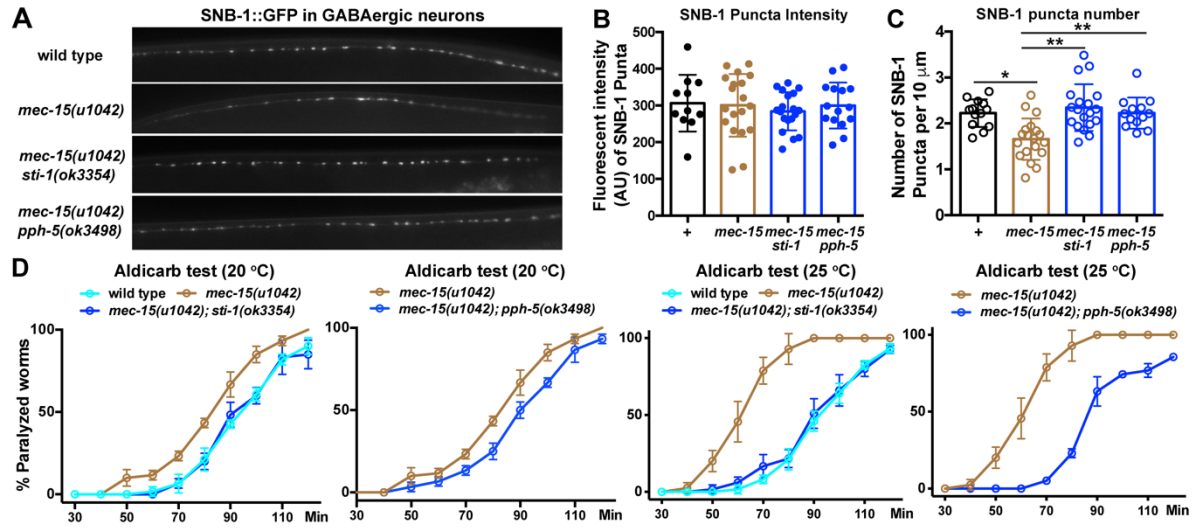

Figure 6

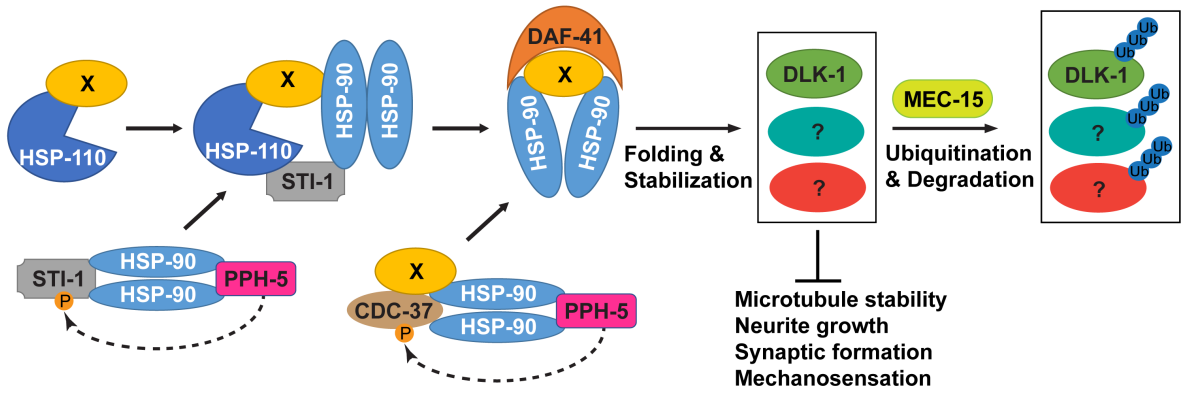
X
HSP-110
X
HSP-110
HSP-90
HSP-90
STI-1
DAF-41
X
HSP-90
HSP-90
Folding &
Stabilization
DLK-1
?
?
MEC-15
Ubiquitination
& Degradation
Ub
DLK-1
?
?
STI-1
HSP-90
HSP-90
PPH-5
P
X
CDC-37
HSP-90
HSP-90
PPH-5
P
Microtubule stability
Neurite growth
Synaptic formation
Mechanosensation

Figure 7